

## **Influence of dual sulfate reduction pathways on pore-fluid chemistry and occurrences of methane hydrate in sediment cores (IODP-353) off Mahanadi basin, Bay of Bengal.**

**A. Peketi<sup>1\*</sup>, A. Mazumdar<sup>1</sup>, S.P.K. Pillutla<sup>1</sup>, D. J. Patil<sup>2</sup>**

<sup>1</sup> Geological Oceanography, CSIR-National Institute of Oceanography, Goa 403004, India

<sup>2</sup> National Geophysical Research Institute, Uppal Road, Hyderabad 500007, India

\*Corresponding author: aditya@nio.org

Phone Number: +91-9850990233

### **Abstract**

Pore fluid chemistry of sediment cores from two coring sites collected from Mahanadi basin (Bay of Bengal) during IODP-353 was studied to understand the intra-basinal variation in microbially mediated sediment biogeochemistry as well as methane hydrate occurrences. The ionic concentrations of  $\text{SO}_4^{2-}$  shows quasi-linear profiles reflecting the steady-state situation in a dominantly diffusion controlled system. Pore-water  $(\Delta\text{TA} + \Delta\text{Ca}^{+2} + \Delta\text{Mg}^{+2})/\Delta\text{SO}_4^{2-}$  ratios and  $\delta^{13}\text{C}_{\text{DIC}}$  depth profiles suggest the influence of dual sulfate reduction pathways (organo-clastic and anaerobic methane oxidation) on the sediment fluid chemistry.  $\delta^{13}\text{C}_{\text{CH}_4}$  values indicate microbial origin of methane. The lowest  $\delta^{13}\text{C}_{\text{CH}_4}$  values in the present study are reported from the sulfate methane transition zone (SMTZ) and attributed to secondary methane generation via microbial recycling of  $^{13}\text{C}$  depleted DIC produced through AOM. Based on the drop in  $\text{Cl}^-$  concentrations relative to the ambient sea-water, we predict the occurrence of disperse/pore-filling methane hydrates in the site U1445 proximal to the basin in which the SMTZ is slightly deeper from the surface compared to the distal (northern) U1446 site.

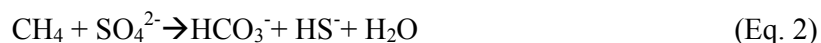
Keywords: Organo clastic sulfate reduction, methane oxidation, dissolved inorganic carbon, IODP, Mahanadi basin.

## Introduction

Organic matter deposited in the marine sediments is re-mineralized by various biogeochemical processes (Schulz and Zabel, 2006) of which, organo-clastic sulfate reduction (OSR) is the leading process that accounts for > 50 % of total organic matter remineralization in marine sediments (Jørgensen, 1982; Canfield, 1989; Kristensen, 2000; Beulig *et al.*, 2018a). Different factors like lability of organic matter, temperature, bacterial species, sedimentation rate, and sulfate concentrations influence the rate of sulfate reduction (Goldhaber and Kaplan, 1975; Westrich and Berner, 1988; Canfield, 1989; Meister *et al.*, 2013). The organo-clastic sulfate reduction is typically represented by equation-1, following Froelich *et al.* (1979).



Anaerobic oxidation of methane (AOM) performed by a consortium of methane-oxidizing archaea (ANME I and II) and sulfate-reducing bacteria (Boetius *et al.*, 2000; Milucka *et al.*, 2012) is also an important pathway responsible for sulfate reduction. AOM takes place within the sulfate-methane transition zone (SMTZ) which typically represent a redox zone within the sediment column, where pore-water sulfate and methane concentration profiles intersect and are markedly depleted due to AOM process (Malinverno and Pohlman, 2011; Mazumdar *et al.*, 2012; Hong *et al.*, 2013; Sultan *et al.*, 2016; Beulig *et al.*, 2018b). Sulfate reduction via AOM pathway can be represented by the stoichiometric equation below (Eq.2).



The sediment column across this redox interface is normally characterized by enhanced concentrations of  $\Sigma\text{HS}^-$  and  $\text{HCO}_3^-$  ions (Ussler and Paull, 2008; Mazumdar *et al.*, 2009a; Mazumdar *et al.*, 2012, Hu *et al.*, 2015; Peketi *et al.*, 2015). The  $\text{HS}^-$  and  $\text{HCO}_3^-$  ionic concentrations are modulated by the precipitation of Fe-sulfides and authigenic carbonates respectively (Ussler and Paull, 2008; Li *et al.*, 2018). The depth of SMTZ below seafloor may vary significantly from <1 to >20 mbsf (Mazumdar *et al.*, 2009b, 2012, 2014; Arning *et al.*, 2015; Graves *et al.*, 2017) which may be attributed to variable diffusive methane flux and sediment permeability. Below the SMTZ, sharp increase in the methane concentrations is commonly attributed to methanogenesis via  $\text{CO}_2$  reduction pathway (Whiticar *et al.*, 1986; Whiticar, 1999; Conrad, 2005; Galimov, 2006). Accumulated methane under suitable pressure-temperature conditions may lead to the formation of methane hydrates within the sediment pores and/or fractures (Kvenvolden, 1993; Sloan, 1998). Formation of methane hydrate may also modify the pore-fluid chemistry (Ussler and Paull, 1995)

e.g., enhanced pore-water chloride concentrations, through salt exclusion; alteration of sediment gas diffusion properties which in turn can also affect the AOM rate (Max, 2003).

The spatial variation in the sediment physical characteristics like porosity, permeability, grain size, and mineralogy as well as organic matter flux can have marked influence on the intrabasinal variation in sediment biogeochemistry reflected in its sediment fluid chemistry (Burdige, 2006; Schluz and Zabel, 2006). Here, we present high-resolution biogeochemical data (head-space gases and pore-waters) from two coring sites (U1445; U1446) in the Mahanadi basin. The major differences between the two coring sites are (i) Site U1445 and U1446 sites are at a water depth of 2513.1 and 1441.2 meters below sea level respectively; (ii) site U1445 is located at the upper rise, whereas U1446 is located at the toe of a northwest-southeast-trending ridge that is part of the strongly incised continental slope and (iii) marginal difference in the sedimentation rates between sites U1445 (~11.4 cm/ky) and U1446 (~16 cm/ky) (Clemens *et al.*, 2016a). The coring operation was carried out on board JOIDES Resolution as part of the IODP-353 expedition. IODP-353 expedition was fundamentally targeted to decipher the past variations in Indian monsoonal activity. However, in view of the large depositional flux of organic matter (Philips *et al.*, 2014; Da Silva *et al.*, 2017), high sedimentation rates, free gas below the bottom simulating reflector (BSR) and reported occurrences of methane gas hydrate (Collett *et al.*, 2008; Mazumdar *et al.*, 2014) underneath, it was thought worthwhile to investigate the intra-basinal variation in sediment pore-fluid biogeochemistry of the cores. The present study contrasts the occurrences of pore-filling methane hydrate at two coring sites as well as the influence of OSR and AOM pathways on pore-water sulfate reduction processes.

## **Geology**

Mahanadi offshore basin is a passive pericratonic basin located along the East coast of India (Singh, 2008), bound by Jagannathpur in the north and Chilka Lake in the south. The 85<sup>0</sup>E Ridge occurring to the south of Lake Chilka forms the approximate south-western limit of the basin. The Mahanadi basin originated in Late Jurassic through the breakup of Gondwana landmass (Sastri *et al.*, 1981). This basin covers an area of ~2,00,000 km<sup>2</sup> of which the offshore component covers an area of 55,000 km<sup>2</sup> (Directorate of Gas and Hydrocarbon; Bastia and Radhakrishna, 2012). The catchment region of the Mahanadi river covers an area of 1,41,589 km<sup>2</sup> (Singh, 2018) and comprises late Archaean and early Proterozoic granite batholiths, tonalite-trondhjemite gneisses, charnockites, khondalites, various sedimentary rocks (limestone, shale, and sandstone) of Gondwana age (Chakrapani and Subramanian, 1990). Mahanadi River along with its tributaries (Shivnath, Jonk, Hasdeo, Barai, Mand, etc.) is the major sediment carrier to the offshore basin, with an annual

sediment loading of  $\sim 7.1 \times 10^6$  tons (Subramanian, 1978). The sediment thickness in this basin varies from 2.9 to 10 km (Subrahmanyam *et al.*, 2008). Reported sedimentation rates calculated using radiocarbon and  $\delta^{18}\text{O}_{G.ruber}$  for the top 40 mbsf varies from 1.5 to 38.6 cm/ky except for the late Holocene sediment package (241.3 cm/ky) (Mazumdar *et al.*, 2014; Phillips *et al.*, 2014; Da Silva *et al.*, 2017). Whereas, biostratigraphy based age dating suggests late Miocene age at the depth of 668 mbsf with an average sedimentation rate of 11.4 cm/ky (Clemens *et al.*, 2016a). The siliciclastic component is dominantly clay-rich with average illite, smectite and (kaolinite + chlorite) contents of  $36.3 \pm 8.6$ ,  $38.5 \pm 11.3$  and  $24.9 \pm 6.7$  % respectively (Mazumdar *et al.*, 2015). The biogenic components comprising  $\text{CaCO}_3$  and total organic carbon (TOC) range from 0.08 to 46.7 and 0.15 to 2.9 wt.% respectively (Da Silva *et al.*, 2017).

## Methodology

Coring operations (Fig. 1) were carried out at sites U1445 (Hole A: Lat.:  $17^\circ 44.7217'$  N, Long.:  $84^\circ 47.2518'$  E; water depth = 2513.1 m, Core recovered = 672 m; Hole B: Lat.:  $17^\circ 44.7098'$  N, Long.:  $84^\circ 47.2498'$  E, water depth = 2514.5 m, core recovered = 33.36 m) and U1446 (Hole A: Lat.:  $19^\circ 05.0090'$  N, Long.:  $85^\circ 44.0894'$  E; water depth = 1441.2 m; core recovered = 180 m. Hole B: Lat.:  $19^\circ 05.0085'$  N, Long.:  $85^\circ 44.0786'$  E; water depth = 1440.5 and core recovered = 27.2 m), where holes 'A' and 'B' were collected for solid phase and fluid phase analyses at variable resolutions. Comprehensive coring protocol and detailed core descriptions are available in Clemens *et al.* (2016b). For fluid analyses, one whole round sediment sample was collected at an interval of 9 m from hole-A, while hole-B was sampled (whole round) at an interval of 1.5 m. Three sediment aliquots were collected in Agilent 20 ml glass vials from each sample for head-space gas concentrations ( $\text{CH}_4$ ,  $\text{C}_2\text{H}_6$ ,  $\text{C}_3\text{H}_8$ ,  $\text{CO}_2$ , and  $\text{H}_2\text{S}$ ) and carbon isotope ratio measurement of  $\text{CH}_4$  and  $\text{CO}_2$ . The ambient air in the sample bottles was removed by flushing with helium and subsequently crimped with butyl rubber septum following the addition of 100  $\mu\text{l}$  of saturated  $\text{HgCl}_2$ . 3 ml of 0.5M NaOH (for  $\text{CO}_2$  absorption) and 100  $\mu\text{l}$  of saturated  $\text{HgCl}_2$  was added to another sediment aliquot for interference free  $\delta^{13}\text{C}_{\text{CH}_4}$  measurements. Carbon dioxide and hydrocarbon gas concentrations were measured on-board JOIDES resolution using a gas chromatograph (Hewlett Packard 6890). The gas concentrations are reported in PPMV following routine IODP protocol (Clemens *et al.*, 2016b). Head space hydrogen sulfide concentrations were determined on-board JOIDES resolution using a gas chromatograph (Hewlett Packard 6890) equipped with a thermal conductivity detector (Clemens *et al.*, 2016b). Carbon isotope ratios of headspace  $\text{CH}_4$  was measured using a Thermo Scientific Delta V Plus continuous flow isotope ratio mass spectrometer coupled to a gas chromatograph (Thermo

trace GC). Natural gas standard-2 (NGS-2: -44.6‰) was used as a reference standard. The external precision of the measurement is typically 0.07-0.09 ‰ VPDB.

In the present report, we have restricted all pore-fluid analyses to a maximum sampling depth of ~222 and 179 mbsf for U1445A and U1446A respectively due to possible contamination of pore-waters by drilling fluid by extended core barrel (XCB) technique used for deeper coring (Zachos *et al.*, 2004). Pore-water from the whole round sediment samples was extracted under nitrogen atmosphere to avoid the oxidation. Following extrusion from the core liner, the outer sediment layer was scraped off to avoid contamination from drilling fluid. The cleaned sediment sample was squeezed to extract pore water using a stainless steel mud squeezer (Manheim and Sayles, 1974) having a diameter of 9 cm. Operational pressure was maintained below 1522 psi which is well below the pressure that could influence the pore water composition (De Lange *et al.*, 1992). Extracted pore-water was filtered through 0.2  $\mu$  disposable syringe filter into 2ml glass vials containing 10  $\mu$ l saturated HgCl<sub>2</sub> for measurement of carbon isotope ratios of dissolved inorganic carbon. The sample vial was filled up to the neck and closed carefully without leaving any air bubbles and stored at 2° C until further measurements. Carbon isotope ratios of dissolved inorganic carbon (DIC) of pore waters was determined with a Thermo Delta V continuous flow isotope ratio mass spectrometer coupled with a GASBENCH II equipped with a PAL auto-sampler at the National geophysical research laboratory (NGRI), Hyderabad (India). IAEA standards NBS-18, NBS-19 and in-house laboratory standards (Carbonate reference standard and MERCK high purity CaCO<sub>3</sub>) were measured multiple times with each batch. The carbon isotope ratios are reported in standard delta notation as permil deviation from the VPDB standard. A sample reproducibility of 0.1 ‰ is reported here.

Pore-water Ca<sup>2+</sup> and Mg<sup>2+</sup> concentrations were determined on-board D/V JOIDES Resolution using an ICP-AES (Teledyne Leeman Prodigy). IAPSO (International Association for the Physical Sciences of the Ocean) seawater standard was used as reference material for calcium and magnesium concentration measurements. The standard deviation (2 $\sigma$ , number of runs = 30) obtained for Ca<sup>2+</sup> and Mg<sup>2+</sup> is 0.72 and 2.02 respectively (Clemens *et al.*, 2016b). Pore-water sulfate and ammonium concentration were measured by ion chromatograph and spectrophotometer respectively on-board the JOIDES Resolution following IODP protocol (Clemens *et al.*, 2016b). Total alkalinity (TA) and chloride concentrations of pore-waters were measured by a Metrohm auto-titrator by means of Gran titration and potentiometric titrations respectively. Few samples were specially collected from mousy sediments for chloride concentration measurements based on physical observation. Porosity was determined by taking ratios of pore water volume and wet volume of the sediment samples (Clemens *et al.*, 2016b). Wet soft sediments were filled in pre-weighed 16 ml wheaton glass vials. Sediments

were dried in convective oven at 105°C for 24 hours and subsequently cooled in desiccator for 3 hours. Wet and dry weights of the sediments were determined using Mettler Toledo electronic balances with a precision of 0.005 g. Dry sample volume was determined using a gas pycnometer system (Micromeritics AccuPyc 1300TC) at 28°C. Volume of pore water was determined based on corrected mass of pore water, pore water density (1.024 g/cm<sup>3</sup>), wet and dry masses of sediments, a ratio of mass constant (0.965 g of fresh water per 1 g of sea water) and weight of evaporated pore water (Blum, 1997).  $\Delta\text{TA}$ ,  $\Delta\text{Ca}^{2+}$ ,  $\Delta\text{Mg}^{2+}$ , and  $\Delta\text{SO}_4^{2-}$  values at each depth interval was calculated by taking the difference between the seawater concentration and pore water concentration at that depth interval of individual parameter respectively. The concentrations of TA, Ca<sup>2+</sup>, Mg<sup>2+</sup>, and SO<sub>4</sub><sup>2-</sup> of seawater are 2.3 mM, 10.3 mM, 53 mM, and 28 mM respectively.

Depth-integrated diffusive flux (J) of sulfate ion for each station was calculated from the pore water sulfate concentration profiles using Fick's First law assuming steady-state conditions (Berner, 1980; Canfield, 1989, 1991),

$$J_{\text{SO}_4} = \phi D_s (dC/dX) \quad (\text{Eq. 3})$$

where J (mmolcm<sup>-2</sup>yr<sup>-1</sup>) is equivalent to the depth-integrated sulfate reduction rate,  $\phi$  is the average porosity, C is the sulfate concentration (mM) in the pore water, dC/dX is the sulfate concentration gradient in mMcm<sup>-1</sup>. 'X' is the depth (cm) from the sediment surface, D<sub>s</sub> (cm<sup>2</sup>sec<sup>-1</sup>) is the molecular diffusivity corrected for tortuosity. D<sub>s</sub> is calculated from the formula,

$$D_s = D_o / (1 + n(1-\phi)) \quad (\text{Eq. 4})$$

Where D<sub>o</sub>=sulfate diffusivity in the absence of particles. Variation in D<sub>o</sub> with temperature is calculated using an empirical relation based on the dataset by Li and Gregory (1974). The calculated D<sub>o</sub> values at U1445B (seabed temperature of 2.45° C) and U1446B (seabed temperature is 5.65° C) are 5.515×10<sup>-6</sup> cm<sup>2</sup>s<sup>-1</sup> and 6.235×10<sup>-6</sup> cm<sup>2</sup>s<sup>-1</sup> respectively assuming n=3 (constant value) for clays and silt (Iversen and Jørgensen, 1993).

Total carbon (TC) and total nitrogen (TN) contents in sediment were determined with an elemental analyzer (Thermo Electron Corporation Flash EA 1112) equipped with a packed column (Thermo Electron) and a thermal conductivity detector on-board JOIDES resolution. La Luna Shale (C=11.52 wt.%) and Thermo soil reference material (33840025) were used as standard reference materials. Repeated analysis of the standard yielded a precision of <0.17%. Total inorganic carbon (TIC) was determined using UIC 5011 CO<sub>2</sub> coulometer on board JOIDES resolution. The calculated precision based on 36 runs is 1%. Organic carbon was determined by subtracting the TIC from TC (Clemens *et al.*, 2016b).

## Results

The head-space methane concentrations of U1445A&B range from 2.1 to 12462.5 ppmv and that of U1446A&B vary from 1.2 to 1517.3 ppmv. At U1445A, ethane concentration ranges from 0.2 to 1.3 ppmv and at U1446A ethane and propane gas concentrations range from 6.7 to 21.6 and 6.9 to 22.9 ppmv respectively. Ethane and propane were not detected in U1445B and U1446B. Very high methane concentrations (up to 1,58,566 ppmv) were recorded from void-gas samples. Measured gas concentrations do not represent the true in-situ concentrations owing to degassing during core recovery (Dickens *et al.*, 1997). Headspace gas concentrations were tabulated in supplementary Table 1. Depth profile of  $\delta^{13}\text{C}_{\text{CH}_4}$  is shown in figure 2. The  $\delta^{13}\text{C}_{\text{CH}_4}$  values at U1445A&B ranges from -109.4 to -68.4 ‰ and that of U1446A&B varies from -98.0 to -70.3 ‰ (supplementary Table 1; Fig. 2A). Most depleted carbon isotope ratios are recorded within or close to the SMTZ. The  $\delta^{13}\text{C}_{\text{CH}_4}$  values show enrichment trend below SMTZ up to a depth of ~53 and 41 mbsf at U1445A and U1446A respectively (Fig. 2A). Below these sediment depths, the isotope ratios fluctuate within a small range (Fig. 2A). Hydrogen sulfide gas (U1445A: 23.2 to 1454.2 and U1446A: 72.3-784 ppmv) was detected only in the void-gas samples (supplementary Table 1).

Pore-water  $\text{SO}_4^{2-}$  concentrations shows linear decreasing trend with depth (bsf) with gradients of 1.4 mM/m and 1.69 mM/m in U1445B and U1446B respectively. Sulfate concentrations decrease to <1 mM within the depth zones of 17-18.5 and 15.6-16.8 mbsf in U1445B and U1446B respectively (Fig. 3). The rise in the head-space methane concentrations starts within the depth zone of 15.5-17 and 14.1-15.6 mbsf at U1445B and U1446B respectively (Fig. 3 A&C). Based on the pore-water sulfate and head space methane concentration profiles, the sulfate-methane transition zones in U1445 and U1446 may be demarcated within the depth-zones of 17 to 18.5 mbsf and 14.1 to 16.8 mbsf respectively (Fig. 3 A&C). The  $J_{\text{SO}_4}$  values for U1445B and U1446B are  $12.2 \pm 0.35$  and  $14.9 \pm 0.31$   $\text{mmolm}^{-2}\text{y}^{-1}$  respectively. The pore-water  $\text{Cl}^-$  concentrations in U1445A remain constant ( $553 \pm 0.5$  mM) within the top 34.7 mbsf; below 35 mbsf, the  $\text{Cl}^-$  concentrations drops steadily to a minimum of 512 mM at 222 mbsf. This trend is superimposed by zones of sharp drop in chloride (260 and 524 mM; Fig. 4). Sharp drops in chloride concentration observed at ~56 and 201 mbsf correspond to the mousy sediments. U1446A has slightly more chloride concentrations (551.4 to 560 mM) compared to that of U1445A, however the former doesn't show a systematic down-depth decrease in chloride

Pore-water TA, calcium and magnesium concentrations are tabulated in supplementary Table 2. In both the sites, alkalinity increases with depth and reaches the maximum values within 40-45 mbsf and 20-25 mbsf (Fig. 5A) in U1445 and U1446 respectively. At U1445A&B and U1446A&B

pore water Ca concentrations decrease linearly within the top 22.5 and 41.5 m respectively, below which it increases with a gentle slope and reaches to a maximum concentration of 4.36 and 4.29 mM at U1445A&B and U1446A&B respectively (Fig. 5B). In both the stations, pore-water Mg concentrations show a decreasing trend with depth (Fig. 5C). Pore-water  $\text{NH}_4^+$  concentration increases with depth at both the sites (Fig. 5D). In U1445A&B  $\text{NH}_4^+$  concentration increases down depth from a core top of 0.24 mM to a maximum value of 7.13 mM at depth 204.87 mbsf (Fig. 5D), whereas, in U1446A&B  $\text{NH}_4^+$  concentration increases down depth from 0.35 to 6.54 mM (Fig. 5D). The vertical profiles of  $\Delta(\text{TA} + \text{Ca}^{2+} + \text{Mg}^{2+})/\Delta(\text{SO}_4^{2-})$  ratios in U1445B and U1446B shows exponential decrease within the top 10 mbsf, below which the ratios (~1.4 and 1.7 in 1445B and U1446B respectively) remain steady with depth (Fig. 6). Carbon isotope ratio profiles of DIC in U1445A&B and U1446A&B show similar trends.  $\delta^{13}\text{C}_{\text{DIC}}$  values initially decrease with depth and show enrichment trend below SMTZ (Fig. 2B). Minimum  $\delta^{13}\text{C}_{\text{DIC}}$  values of -31.5 and -34.5 ‰ are recorded within the SMTZs of U1445B and U1446B respectively. Below the SMTZ, the  $\delta^{13}\text{C}_{\text{DIC}}$  values increase asymptotically to near steady-state values of ~ 8 to 9 ‰ (Fig. 2B).

Total organic carbon (TOC) varies from 0.8-2.26 and 0.8 to 2.9 (wt. %) at U1445A and U1446A respectively. At U1445A, total inorganic carbon (TIC) varies from 0.13-2.99 except with a high TIC content of 6.1 wt. % at ~99 mbsf, at U1446A it varies from 0.073 to 2.38 (wt. %). Total nitrogen content varies from and 0.21 to 0.44 and 0.25 to 0.94 wt. % at U1445A and U1446A respectively (supplementary Table 3).

## Discussion

### AOM and OSR: Dual sulfate reduction pathways

In U1445B and U1446B, the pore-water sulfate concentrations decrease quasi-linearly with depth below the seafloor (Fig. 3). The quasi-linear sulfate concentration profile reflects a steady-state situation in a diffusion dominated system (Hensen *et al.*, 2003; Mazumdar *et al.*, 2014). In contrast, a fracture/advection dominated system shows kink, concave and sigmoidal transient sulfate concentration profiles which essentially represent upward advective methane flux (Mazumdar *et al.*, 2012) and/or slide events (Zabel and Schulz, 2001). The calculated  $J_{\text{SO}_4}$  values (12.2 and 14.9  $\text{mmolm}^{-2}\text{y}^{-1}$  at U1445B and U1446B respectively) are close to the previously reported  $J_{\text{SO}_4}$  values (10.2 to 12.8  $\text{mmolm}^{-2}\text{y}^{-1}$ ) from the Mahanadi offshore (Mazumdar *et al.*, 2014). The  $J_{\text{SO}_4}$  values in marine organic rich sediment are the net result of OSR and AOM driven sulfate reduction processes. Organo-clastic sulfate reduction and AOM processes depend on the concentrations of low molecular weight organic molecules like lactate/formate, acetate, methyl alcohol, etc. (fermentation products:



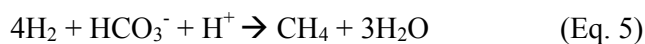
Jørgensen and Kasten, 2006) amenable to the sulfate reducers; diffusive/advective methane flux and distribution of sulfate reducers and methanotrophs in the sediments (Zabel and Schulz, 2001; Kastner *et al.*, 2008, Mazumdar *et al.*, 2012; Fernandes *et al.*, 2018). The amenability of labile organic molecules to the sulfate reducers further depends on sedimentation rate (Canfield, 1989; Lin *et al.*, 2002), bottom water oxygen concentrations (Burdige, 2007; Nierop *et al.*, 2017), organic-matter flux (Canfield, 1989), and bioturbation activity of benthic biota (Kristensen, 2000). On the other hand, methane flux is governed by the activity of methanogens (Ferry, 1992) and sediment permeability (Treude and Ziebis, 2010). The  $\Delta(\text{TA} + \text{Ca}^{2+} + \text{Mg}^{2+})/\Delta\text{SO}_4^{2-}$  ratio profile is a reasonable indicator of the relative influence of OSR and AOM processes on fluid chemistry (Kulm *et al.*, 1986; Claypool *et al.*, 2006; Kastner *et al.*, 2008; Chen *et al.*, 2010; Hu *et al.*, 2015). An AOM driven sulfate reduction process results in  $\Delta(\text{TA} + \text{Ca}^{2+} + \text{Mg}^{2+})/\Delta\text{SO}_4^{2-}$  ratio of 1:1, whereas, this ratio is  $\sim 2:1$  where OSR is the driver for sulfate reduction. Except few high ratios ( $>2:1$ ) observed within the top 3 mbsf (Fig. 6) remaining ratios are within the end member ratios of 1:1 and 2:1 indicating dual influence of AOM and OSR in both the cores. The decrease in  $\Delta(\text{TA} + \text{Ca}^{2+} + \text{Mg}^{2+})/\Delta\text{SO}_4^{2-}$  ratios in U1446B towards the SMTZ further suggest the increasing influence of AOM on the sulfate concentration gradient. Higher  $J_{\text{SO}_4}$ , shallower depth of SMTZ in U1446B compared to that of U1445B may also be attributed to stronger AOM in the former.

The dual effect of OSR and AOM on sulfate concentration gradient (or  $J_{\text{SO}_4}$ ) is also evident from the pore-water  $\delta^{13}\text{C}_{\text{DIC}}$  values. DIC in the sediment pore-waters can have multiple sources including seawater, and bicarbonate produced via OSR and AOM processes (Eq. 1 and 2). The steady decrease in  $\delta^{13}\text{C}_{\text{DIC}}$  values from the seabed towards the SMTZ is attributed to the addition of DIC as a product of OSR and AOM. Since the carbon isotope fractionation during the organic matter oxidation to  $\text{CO}_2$  is low (Blair *et al.*, 1994), the end member  $\delta^{13}\text{C}_{\text{DIC}}$  values of the DIC produced via OSR pathway is expected to be close to the  $\delta^{13}\text{C}$  values (-22.3 to -16.3 ‰) of the organic carbon in the Mahanadi sediments (Philips *et al.*, 2014; Da Silva *et al.*, 2017). In both the sites the lowest  $\delta^{13}\text{C}_{\text{DIC}}$  values (-34.5‰ in [U1446] and -31.5 ‰ in [U1445]; Fig. 2B) are within the SMTZ attributed to AOM. AOM pathway within the SMTZ (Eq. 2) is expected to produce bicarbonate having carbon isotope ratios  $\sim 5$  to 30 ‰ (Whiticar and Faber, 1986; Whiticar, 1999; Wehrmann *et al.*, 2011) enriched relative to the isotopic ratio of the residual methane which ranges from -109 to -98.7 ‰ (Fig. 2). However, the measured  $\delta^{13}\text{C}_{\text{DIC}}$  values show marked  $^{13}\text{C}$  enrichment suggesting a significant contribution of DIC produced via OSR pathway. This observation is supported by Komada *et al.* (2016) and Wu *et al.* (2016) who reported 35 to 45 % and 50 to 66.7 % of sulfate reduction via OSR pathway within SMTZ. Based on the range of  $\delta^{13}\text{C}_{\text{DIC}}$  values within the SMTZ,

U1446 shows greater DIC contribution from AOM compared to that of U1445. Above SMTZ, the steady increase in  $\delta^{13}\text{C}_{\text{DIC}}$  values towards the core top indicates the increasing influence of sea-water derived DIC (-4 to -1‰ from the Bay of Bengal; Sherin *et al.*, 2018) in the sediment pore-waters compared to the DIC contribution from OSR and AOM processes (Chuang *et al.*, 2019). Whereas, the marked increase in  $\delta^{13}\text{C}_{\text{DIC}}$  values (Fig. 2B) below the SMTZ can be attributed to the carbon isotopic fractionation due to methanogenesis following  $\text{CO}_2$  reduction pathway (Whiticar, 1999; Paull *et al.*, 2000; Galimov, 2006; Wehrmann *et al.*, 2011). Down-depth increase in the  $\text{NH}_4^+$  concentrations (Fig. 5D) across the SMTZ is a reliable indicator of microbially mediated organic matter degradation (Cranston, 1991) which also supports OSR processes. Pore water ammonium concentration is influenced by limited processes such as adsorption of ammonium on to solid phases like clay particles, organic particulates and Fe-oxyhydroxides (Muller, 1977).

### **Methanogenesis**

Highly depleted carbon isotope ratios of methane (-109.3 to -68 ‰) across the sediment cores (Fig. 2A) suggest methanogenesis via microbial reduction of  $\text{CO}_2$  (Whiticar and Faber, 1986; Whiticar, 1999; Galimov, 2006). Lowest  $\delta^{13}\text{C}_{\text{CH}_4}$  values recorded within the SMTZ is counter-intuitive since high rate of methanotrophy would suggest enrichment of residual methane (Whiticar, 1999). The recorded  $^{13}\text{C}$  depletion may be attributed to secondary methane generation (Eq. 5) via microbial recycling of  $^{13}\text{C}$  depleted DIC produced through AOM (Yoshinaga *et al.*, 2014, Geprags *et al.*, 2016). However, the contribution of this methane does not significantly increase the methane concentration (Geprags *et al.*, 2016). A recent study by Chuang *et al.* (2019) by means of field data and model simulations attributed lowest  $\delta^{13}\text{C}_{\text{CH}_4}$  and  $\delta^{13}\text{C}_{\text{DIC}}$  values within SMTZ to carbon isotope equilibrium during AOM.



Below SMTZ, methane shows an enrichment trend with depth which can be attributed to the preferential conversion of isotopically lighter  $\text{CO}_2$  to methane during methanogenesis. Carbon isotope ratio profile of DIC also shows a similar pattern to that of methane with most depleted ratios within the SMTZ (Fig. 2).

### **Signature of methane hydrate and free gas in the sediment**

The fluctuation in the pore-water chloride concentrations is commonly attributed to freshwater induced dilution due to thawing of methane hydrate, illitization of smectite and/or opal-A to opal CT transformation (Kastner *et al.*, 1977; Suess, 2014). The latter two processes may be considered as in situ dilutions in contrast to post-core recovery dilution artifact caused by hydrate dissociation. On the

other hand, salt exclusion caused by methane hydrate crystallization causes pockets of enhanced salinity exceeding ambient sea water values. In U1445A, the steady drop in the chloride concentrations is superimposed by two sharp spikes (Fig. 4). The dilution observed here is most likely induced by fresh water release due to post- coring methane hydrate thawing, since illitization of smectite and opal-A to opal-CT conversion which releases fresh water in situ is expected to take place at considerably higher P-T conditions than what the present cores are subjected to (water depth = 2500 mbsl, sea bed temperature = 2.45° C and GTG = 52° C/km: Collett *et al.*, 2008; Clemens *et al.*, 2016a). Based on seismic data, drilling & well logging activities, geochemical and physical studies, existence of disseminated gas hydrate has been reported from Mahanadi basin (Collett *et al.*, 2008). Collett *et al.* (2012) observed the presence of several small IR thermal anomalies (shift to colder values) coupled with subtle pore water freshening and attributed these variations to the presence of minor quantities for disseminated gas hydrate. It is important to note that no fresh water-induced Cl<sup>-</sup> dilution is observed in U1446 (W.D 1432 mbsl, seabed temp = 5.65°C). This may be attributed to lack of methane hydrate formation in U1446 compared to a regular increase in grain pore-filling methane hydrate in U1445 with depth below the seafloor. The low Cl<sup>-</sup> concentration spikes at 56.6 and 200.6 mbsf (Fig. 4) in U1445 possibly indicate hydrate filled veinlets/pockets due to focused crystallization within a fracture system. The calculated depth (Maekawa *et al.*, 1995; Miles, 1995; Collett *et al.*, 2008) of gas hydrate stability zone (GHSZ) at U1445 and U1446 are 699 and 309 mbsf respectively. One of the possible reasons for the absence of pore-filling methane hydrate in U1446 compared to that of U1445 is possibly lack of sufficient methane flux for hydrate synthesis. This is also evident from the order of magnitude lower methane concentrations in U1446 compared to that of U1445 (Fig. 3). In spite of significantly lower methane concentrations, a higher contribution of AOM towards sulfate reduction is noticeable in U1446, which may be attributed to microbial ecology and sediment permeability.

## Conclusion

1. The quasi-linear sulfate concentration profile reflects a steady-state situation in a diffusion controlled system.
2.  $\Delta(\text{TA} + \text{Ca}^{2+} + \text{Mg}^{2+}) / \Delta\text{SO}_4^{2-}$  and  $\delta^{13}\text{C}_{\text{DIC}}$  values suggest the influence of both AOM and OSR on sulfate concentration gradient in both the cores. The  $\delta^{13}\text{C}_{\text{DIC}}$  values within the SMTZ are significantly higher than what is expected in solely AOM driven sulfate reduction indicating a notable contribution of OSR process within the SMTZ. Shallower SMTZ and lower  $\delta^{13}\text{C}_{\text{DIC}}$  values in U1446B suggest greater AOM activity compared to that of U1445B.

3. The depth-wise drop in chloride (Cl<sup>-</sup>) concentrations superimposed by low concentration spikes in the core U1445 is attributed to a possible presence of pore filling methane hydrate compared to that of U1446 which does not show any chloride concentration anomaly. The possibility of methane hydrate occurrences in U1445 is also supported by high headspace methane concentrations and thicker GHSZ compared to that of U1446.

### **Acknowledgments**

We thank the directors of NIO and NGRI, for supporting this study. We thank IODP (Expedition party 353) for providing samples. We thank Steven C. Clemens, Wolfgang Kuhnt Co-Chief Scientists, Leah J. LeVay (Expedition Project Manager), Ed C. Hathorne (GEOMAR Helmholtz Centre for Ocean Research Kiel), Yongsong Huang Organic Geochemist (Department of Earth, Environmental, and Planetary Sciences Brown University), John B. Kirkpatrick (University of Rhode Island), Netramani Sagar (National Geophysical Research Institute), Masanobu Yamamoto (Hokkaido University) for support and data generation in geochemistry laboratory, onboard JOIDES resolution. We thank Dr. Collett for providing the software to calculate the gas hydrate stability zone. Comments and suggestions from the reviewers are sincerely acknowledged. We sincerely thank IODP India for funding the program.

### **References:**

- Arning, E. T., Gaucher, E. C., van Berk, W. and Schulz, H.-M. (2015) Hydrogeochemical models locating sulfate-methane transition zone in marine sediments overlying black shales: A new tool to locate biogenic methane? *Marine and Petroleum Geology*. **59**, 563-574.
- Bastia, R. and Radhakrishna, M. (2012) *Basin evolution and petroleum prospectivity of the continental margins of India*. Elsevier
- Beulig, F., Roy, H., Glombitza, C. and Jørgensen, B. B. (2018a) Control on rate and pathway of anaerobic organic carbon degradation in the seabed. *Proceedings of the National Academy of Sciences*. 201715789.
- Beulig, F., Roy, H., McGlynn, S. E. and Jørgensen, B. B. (2018b) Cryptic CH<sub>4</sub> cycling in the sulfate-methane transition of marine sediments apparently mediated by ANME-1 archaea. *ISME J*. **296**, 10.1038.
- Blair, N. E., Plaia, G. R., Boehme, S. E., DeMaster, D. J. and Levin, L. A. (1994) The remineralization of organic carbon on the North Carolina continental slope. *Deep Sea Research Part II: Topical Studies in Oceanography*. **41**, 755-766.

- Blum, P., 1997. Technical Note 26: Physical Properties Handbook—A guide to the Shipboard Measurement of Physical Properties of Seep-sea Cores. *Ocean Drilling Program*.
- Boetius, A., Ravenschlag, K., Schubert, C. J., Rickert, D., Widdel, F., Giesecke, A., Amann, R., Jørgensen, B. B., Witte, U., Pfannkuche, O. (2000) A marine microbial consortium apparently mediating anaerobic oxidation of methane. *Nature*. **407**, 623– 626.
- Burdige, D. J. (2006) *Geochemistry of marine sediments*. Princeton university press, 609 pp.
- Burdige, D. J. (2007) Preservation of organic matter in marine sediments: controls, mechanisms, and an imbalance in sediment organic carbon budgets? *Chemical reviews*. **107**, 467-485.
- Canfield, D. E. (1989) Sulfate reduction and oxic respiration in marine sediments: implications for organic carbon preservation in euxinic environments. *Deep Sea Research Part A. Oceanographic Research Papers*. **36**, 121-138.
- Canfield, D. E. (1991) Sulfate reduction in deep-sea sediments. *American Journal of Science*. **291**, 177-188.
- Chakrapani, G. J. and Subramanian, V. (1990) Preliminary studies on the geochemistry of the Mahanadi river basin, India. *Chemical Geology*. **81**, 241-253.
- Chuang, P.-C., Yang, T. F., Wallmann, K., Matsumoto, R., Hu, C.-Y., Chen, H.-W., Lin, S., Sun, C.-H., Li, H.-C. and Wang, Y. (2019) Carbon isotope exchange during anaerobic oxidation of methane (AOM) in sediments of the northeastern South China Sea. *Geochimica et Cosmochimica Acta*. **246**, 138-155.
- Chen, Y., W. Ussler Iii, H. Haflidason, A. Lepland, L. Rise, M. Hovland, and B. O. Hjelstuen (2010), Sources of methane inferred from pore-water  $\delta^{13}\text{C}$  of dissolved inorganic carbon in Pockmark G11, offshore Mid-Norway, *Chemical Geology*, **275(3)**, 127-138.
- Claypool, G. E., A. V. Milkov, Y.-J. Lee, M. E. Torres, W. S. Borowski, and H. Tomaru (2006), Microbial methane generation and gas transport in shallow sediments of an accretionary complex, southern Hydrate Ridge (ODP Leg 204), offshore Oregon, USA, *Proceedings of the Ocean Drilling Program, Scientific Results*, **204**, 1-52.
- Clemens, S. C., Kuhnt, W., LeVay, L. J., Anand, P., Ando, T., Bartol, M., Bolton, C. T., Ding, X., Gariboldi, K., Giosan, L., E.C. Hathorne, Y. Huang, P. Jaiswal, S. Kim, J.B. Kirkpatrick, K. Littler, G. Marino, P. Martinez, D. Naik, A. Peketi, S.C. Phillips, M.M. Robinson, O.E. Romero, N. Sagar, K.B. Taladay, S.N. Taylor, K. Thirumalai, G. Uramoto, Y. Usui, J. Wang, M. Yamamoto and Zhou, L. (2016a) Expedition 353 summary. **353**.
- Clemens, S. C., Kuhnt, W., LeVay, L.J., and the Expedition 353 Scientists. (2016b) Expedition methods. *Proc. IODP*. **353**.
- Collett, T., Riedel, M., Cochran, J., Boswell, R., Presley, J., Kumar, P., Sathe, A., Sethi, A., Lall, M. and Sibal, V. (2008) Indian National Gas Hydrate Program: Expedition 01, Initial Reports, vol. 1, Dir. Gen. of Hydrocarbon, New Delhi, India.
- Collett, T. S., M. Riedel, J. Cochran, R. Boswell, J. Presley, P. Kumar, A. Sathe, A. Sethi, M. Lall, and E. S. NGHP (2012) Indian national gas hydrate program expedition 01 report, US Department of the Interior, US Geological Survey.

- Conrad, R. (2005) Quantification of methanogenic pathways using stable carbon isotopic signatures: a review and a proposal. *Organic Geochemistry*. **36**, 739-752.
- Cranston, R. E. (1991) Sedimentation rate estimates from sulfate and ammonia gradients. In: Barron, J., et al. (Eds.), Proceedings of the Ocean Drilling Program, Scientific Results, vol. 119. pp. 401-405.
- Da Silva, R., Mazumdar, A., Mapder, T., Peketi, A., Joshi, R. K., Shaji, A., Mahalakshmi, P., Sawant, B., Naik, B. G. and Carvalho, M. A. (2017) Salinity stratification controlled productivity variation over 300 ky in the Bay of Bengal. *Scientific reports*. **7**, 14439.
- De Lange, G. J., Cranston, R. E., Hydes, D. H. and Boust, D. (1992) Extraction of pore water from marine sediments: a review of possible artifacts with pertinent examples from the North Atlantic. *Marine Geology*. **109**, 53-76.
- Dickens, G. R., Paull, C. K. and Wallace, P. (1997) Direct measurement of in situ methane quantities in a large gas-hydrate reservoir. *Nature*. **385**, 426-428.
- Fernandes, S., Mazumdar, A., Bhattacharya, S., Peketi, A., Mapder, T., Roy, R., Carvalho, M. A., Roy, C., Mahalakshmi, P. and Silva, R. (2018) Enhanced carbon-sulfur cycling in the sediments of Arabian Sea oxygen minimum zone center. *Scientific reports*. **8**, 8665.
- Ferry, J. G. (1992) Biochemistry of methanogenesis. *Critical reviews in biochemistry and molecular biology*. **27**, 473-503.
- Froelich, P., Klinkhammer, G., Bender, M., Luedtke, N., Heath, G., Cullen, D., Dauphin, P., Hammond, D., Hartman, B. and Maynard, V. (1979) Early oxidation of organic matter in pelagic sediments of the eastern equatorial Atlantic: suboxic diagenesis. *Geochimica et Cosmochimica Acta*. **43**, 1075-1090.
- Galimov, E. (2006) Isotope organic geochemistry. *Organic Geochemistry*. **37**, 1200-1262.
- Gepreghs, P., Torres, M. E., Mau, S., Kasten, S., Romer, M. and Bohrmann, G. (2016) Carbon cycling fed by methane seepage at the shallow Cumberland Bay, South Georgia, sub-Antarctic. *Geochemistry, Geophysics, Geosystems*. **17**, 1401-1418.
- Goldhaber, M. and Kaplan, I. (1975) Controls and consequences of sulfate reduction rates in recent marine sediments. *Soil Science*. **119**, 42-55.
- Graves, C. A., James, R. H., Sapart, C. J., Stott, A. W., Wright, I. C., Berndt, C., Westbrook, G. K. and Connelly, D. P. (2017) Methane in shallow subsurface sediments at the landward limit of the gas hydrate stability zone offshore western Svalbard. *Geochimica et Cosmochimica Acta*. **198**, 419-438.
- Hensen, C., Zabel, M., Pfeifer, K., Schwenk, T., Kasten, S., Riedinger, N., Schulz, H. and Boetius, A. (2003) Control of sulfate pore-water profiles by sedimentary events and the significance of anaerobic oxidation of methane for the burial of sulfur in marine sediments. *Geochimica et Cosmochimica Acta*. **67**, 2631-2647.
- Hong, W.-L., Torres, M. E., Kim, J.-H., Choi, J. and Bahk, J.J. (2013) Carbon cycling within the sulfate-methane-transition-zone in marine sediments from the Ulleung Basin. *Biogeochemistry*. **115**, 129-148.

- Hu, Y., Feng, D., Liang, Q., Xia, Z., Chen, L. and Chen, D. (2015) Impact of anaerobic oxidation of methane on the geochemical cycle of redox-sensitive elements at cold-seep sites of the northern South China Sea. *Deep Sea Research Part II: Topical Studies in Oceanography*. **122**, 84-94.
- Iversen, N. and Jørgensen, B. B. (1993) Diffusion coefficients of sulfate and methane in marine sediments: influence of porosity. *Geochimica et Cosmochimica Acta*. **57**, 571-578.
- Jørgensen, B. (1982) Mineralization of organic matter in the sea bed—the role of sulphate reduction. *Nature*. 643-645.
- Jørgensen, B. and Kasten, S. (2006) Sulfur cycling and methane oxidation. *Marine geochemistry*, 271-309, Springer.
- Kastner, M., Keene, J. B. and Gieskes, J. M. (1977) Diagenesis of siliceous oozes-I. Chemical controls on the rate of opal-A to opal-CT transformation-an experimental study. *Geochimica et Cosmochimica Acta*. **41**, 1041-1059.
- Kastner, M., Claypool, G. and Robertson, G. (2008) Geochemical constraints on the origin of the pore fluids and gas hydrate distribution at Atwater Valley and Keathley Canyon, northern Gulf of Mexico. *Marine and Petroleum Geology*. **25**, 860-872.
- Komada, T., Burdige, D. J., Li, H.-L., Magen, C., Chanton, J. P. and Cada, A. K. (2016) Organic matter cycling across the sulfate-methane transition zone of the Santa Barbara Basin, California Borderland. *Geochimica et Cosmochimica Acta*. **176**, 259-278.
- Kristensen, E. (2000) Organic matter diagenesis at the oxic/anoxic interface in coastal marine sediments, with emphasis on the role of burrowing animals. *Hydrobiologia*. **426**, 1-24.
- Kulm, L. D., E. Suess, J. C. Moore, B. Carson, B. T. Lewis, S. D. Ritger, D. C. Kadko, T. M. Thornburg, R. W. Embley, and W. D. Rugh (1986) Oregon subduction zone: venting, fauna, and carbonates, *Science*, **231**(4738), 561-566.
- Kvenvolden, K. (1993) Gas hydrates—geological perspective and global change. *Reviews of Geophysics*. **31**, 173–187.
- Li, Y. H. and Gregory, S. (1974) Diffusion of ions in sea water and in deep-sea sediments. *Geochimica et Cosmochimica Acta*. **38**, 703-714.
- Li, J., Peng, X., Bai, S., Chen, Z. and Van Nostrand, J. D. (2018) Biogeochemical processes controlling authigenic carbonate formation within the sediment column from the Okinawa Trough. *Geochimica et Cosmochimica Acta*. **222**, 363-382.
- Lin, S., Huang, K. M. and Chen, S. K. (2002) Sulfate reduction and iron sulfide mineral formation in the southern East China Sea continental slope sediment. *Deep Sea Research Part I: Oceanographic Research Papers*. **49**, 1837-1852.
- Maekawa, T., Itoh, S., Sakata, S., Igari, S. i. and Imai, N. (1995) Pressure and temperature conditions for methane hydrate dissociation in sodium chloride solutions. *Geochemical Journal*. **29**, 325-329.

- Malinverno, A. and Pohlman, J. W. (2011) Modeling sulfate reduction in methane hydrate-bearing continental margin sediments: Does a sulfate-methane transition require anaerobic oxidation of methane? *Geochemistry Geophysics Geosystems*. **12**, Q07006.
- Manheim, F. T. and Sayles, F. L. (1974) Composition and origin of interstitial waters of marine sediments, based on deep sea drill cores. In Goldberg, E.D. (Ed.), *The Sea (Vol. 5): Marine Chemistry: The Sedimentary Cycle*: New York (Wiley), 527–568.
- Max, M. D. (2003) *Natural gas hydrate in oceanic and permafrost environments*. Springer Science & Business Media, 415 pp.
- Mazumdar, A., Dewangan, P., João, H. M., Peketi, A., Khosla, V., Kocherla, M., Badesab, F. K., Joshi, R. K., Roxanne, P. and Ramamurty, P. B. (2009a) Evidence of paleo–cold seep activity from the Bay of Bengal, offshore India. *Geochemistry Geophysics Geosystems*. **10**, Q06005.
- Mazumdar, A., Peketi, A., Dewangan, P., Badesab, F., Ramprasad, T., Ramana, M. V., Patil, D., J., and Dayal, A. (2009b) Shallow gas charged sediments off the Indian west coast: Genesis and distribution. *Marine Geology*. **267**, 71-85.
- Mazumdar, A., H.M. Joao, A. Peketi, P. Dewangan, M. Kocherla, R.K. Joshi and Ramprasad, T. (2012) Geochemical and geological constraints on the composition of marine sediment pore fluid: Possible link to gas hydrate deposits. *Marine and Petroleum Geology*. **38**, 35-52.
- Mazumdar, A., Peketi, A., Joao, H. M., Dewangan, P. and Ramprasad, T. (2014) Pore-water chemistry of sediment cores off Mahanadi Basin, Bay of Bengal: Possible link to deep seated methane hydrate deposit. *Marine and Petroleum Geology*. **49**, 162-175.
- Mazumdar, A., Kocherla, M., Carvalho, M. A., Peketi, A., Joshi, R. K., Mahalaxmi, P., Joao, H. M. and Jisha, R. (2015) Geochemical characterization of the Krishna-Godavari and Mahanadi offshore basin (Bay of Bengal) sediments: A comparative study of provenance. *Marine and Petroleum Geology*. **60**, 18-33.
- Meister, P., Liu, B., Ferdelman, T.G., Jørgensen, B.B., and Khalili, A. (2013) Control of sulphate and methane distributions in marine sediments by organic matter reactivity. *Geochimica et Cosmochimica Acta*. **104**, 183-193.
- Miles, P. R. (1995) Potential distribution of methane hydrate beneath the European continental margins. *Geophysical Research Letters*, **22**, 3179-3182.
- Milucka, J., Ferdelman, T. G., Polerecky, L., Franzke, D., Wegener, G., Schmid, M., Lieberwirth, I., Wagner, M., Widdel, F. and Kuypers, M. M. (2012) Zero-valent sulphur is a key intermediate in marine methane oxidation. *Nature*. **491**, 541-546.
- Muller, P. J. (1977) C/N ratios in Pacific deep-sea sediments: Effect of inorganic ammonium and organic nitrogen compounds sorbed by clays. *Geochimica et Cosmochimica Acta*. **41**, 765-776.
- Nierop, K. G. J., Reichart, G.-J., Veld, H. and Damste, J. S. S. (2017) The influence of oxygen exposure time on the composition of macromolecular organic matter as revealed by surface sediments on the Murray Ridge (Arabian Sea). *Geochimica et Cosmochimica Acta*. **206**, 40-56.



- Paull, C. K., Lorenson, T. D., Borowski, W. S., Ussler III, W., Olsen, K. and Rodriguez, N. M. (2000) Isotopic composition of CH<sub>4</sub>, CO<sub>2</sub> species, and sedimentary organic matter within samples from the Blake Ridge: Gas source implications. *Proc. ODP, Sci. Results*. 67-78.
- Peketi, A., Mazumdar, A., Joao, H. M., Patil, D. J., Usapkar, A. and Dewangan, P. (2015) Coupled C-S-Fe geochemistry in a rapidly accumulating marine sedimentary system: Diagenetic and depositional implications. *Geochemistry, Geophysics, Geosystems*. **16**.
- Phillips, S. C., Johnson, J. E., Giosan, L. and Rose, K. (2014) Monsoon-influenced variation in productivity and lithogenic sediment flux since 110 ka in the offshore Mahanadi Basin, northern Bay of Bengal. *Marine and Petroleum Geology*. **58**, 502-525.
- Sastri, V., Venkatachala, B. and Narayanan, V. (1981) The evolution of the east coast of India. *Palaeogeography, Palaeoclimatology, Palaeoecology*. **36**, 23-54.
- Schulz, H. D. and Zabel, M. (2006) *Marine geochemistry*. Springer Verlag, 574 pp.
- Sherin, C. K., Sarma, V., Rao, G. D., Viswanadham, R., Omand, M. M., and Murty, V. S. N. (2018) New to total primary production ratio (f-ratio) in the Bay of Bengal using isotopic composition of suspended particulate organic carbon and nitrogen, *Deep Sea Research Part I: Oceanographic Research Papers*, **139**, 43-54.
- Singh, L. (2008) *Oil and gas fields of India*. Indian Petroleum Publishers, 382 pp.
- Singh, D. S. (2018) *The Indian Rivers: Scientific and Socio-economic Aspects*. Springer, 551 pp.
- Sloan, E. (1998) *Clathrate hydrates of natural gases*. CRC Press, 705 pp.
- Subramanian, V. (1978) Input by Indian rivers into the world oceans. *Proceedings of the Indian Academy of Sciences-Section A, Earth and Planetary Sciences*. **87**, 77-88.
- Subrahmanyam, V., Subrahmanyam, A. S., Murty, G. P. S. and Murthy, K. S. R. (2008) Morphology and tectonics of Mahanadi Basin, northeastern continental margin of India from geophysical studies. *Marine Geology*. **253**, 63-72.
- Suess, E. (2014) Marine cold seeps and their manifestations: geological control, biogeochemical criteria and environmental conditions. *International Journal of Earth Sciences*. **103**, 1889-1916.
- Sultan, N., Garziglia, S. b. and Ruffine, L. (2016) New insights into the transport processes controlling the sulfate-methane-transition-zone near methane vents. *Scientific reports*. **6**, serp26701.
- Treude, T. and Ziebis, W. (2010) Methane oxidation in permeable sediments at hydrocarbon seeps in the Santa Barbara Channel, California. *Biogeosciences (BG)*. **7**, 3095-3108.
- Ussler III, W. and Paull, C. (1995) Effects of ion exclusion and isotopic fractionation on pore water geochemistry during gas hydrate formation and decomposition. *Geo-marine letters*. **15**, 37-44.

- Ussler III, W. and Paull, C. K. (2008) Rates of anaerobic oxidation of methane and authigenic carbonate mineralization in methane-rich deep-sea sediments inferred from models and geochemical profiles. *Earth and Planetary Science Letters*. **266**, 271-287.
- Wehrmann, L. M., Risgaard-Petersen, N., Schrum, H. N., Walsh, E. A., Huh, Y., Ikehara, M., Pierre, C., D'Hondt, S., Ferdelman, T. G. and Ravelo, A. C. (2011) Coupled organic and inorganic carbon cycling in the deep subseafloor sediment of the northeastern Bering Sea Slope (IODP Exp. 323). *Chemical Geology*. **284**, 251-261.
- Westrich, J. and Berner, R. (1988) The effect of temperature on rates of sulfate reduction in marine sediments. *Geomicrobiology Journal*. **6**, 99-117.
- Whiticar, M. J., Faber, E. and Schoell, M. (1986) Biogenic methane formation in marine and freshwater environments: CO<sub>2</sub> reduction vs. acetate fermentation--isotope evidence. *Geochimica et cosmochimica acta*. **50**, 693-709.
- Whiticar, M. J. (1999) Carbon and hydrogen isotope systematics of bacterial formation and oxidation of methane. *Chemical Geology*. **161**, 291-314.
- Wu, Z., Zhou, H., Ren, D., Gao, H. and Li, J. (2016) Quantifying the sources of dissolved inorganic carbon within the sulfate-methane transition zone in near shore sediments of Qi'ao Island, Pearl River Estuary, Southern China. *Science China Earth Sciences*. 1-12.
- Yoshinaga, M. Y., Holler, T., Goldhammer, T., Wegener, G., Pohlman, J. W., Brunner, B., Kuypers, M. M. M., Hinrichs, K.-U. and Elvert, M. (2014) Carbon isotope equilibration during sulphate-limited anaerobic oxidation of methane. *Nature Geoscience*. **7**, 190-194.
- Zabel, M. and Schulz, H. D. (2001) Importance of submarine landslides for non-steady state conditions in pore water system-lower Zaire (Congo) deep-sea fan. *Marine Geology*. **176**, 87-99.
- Zachos, J. C., Kroon, D., Blum, P., Bowles, J., Gaillot, P., Hasegawa, T. and Hathorne, E. C. (2004) Proceedings of the Ocean Drilling Program, Initial Reports, Volume 208.

**Figure captions:**

**Figure 1:** Coring sites of Expedition 353 (modified after Clemens *et al.*, .2016a). U1445 and U1446 sites are highlighted in red-colored rectangular box.

**Figure 2:** Carbon isotope ratios of headspace CH<sub>4</sub>, and dissolved inorganic carbon (DIC) of cores U1445A&B and U1446A&B.

**Figure 3:** Depth wise sulfate, alkalinity, and methane concentration profiles. Blue shaded zone indicates sulfate methane transition zone (SMTZ) and dotted lines indicate sulfate methane interface.

**Figure 4:** Depth wise pore water chloride concentrations of U1445A and U1446A, marked with sharp chloride spikes.

**Figure 5:** Depth wise total alkalinity, Ca<sup>2+</sup>, Mg<sup>2+</sup> and NH<sub>4</sub><sup>+</sup> concentration profiles of cores U1445A&B and U1446A&B.

**Figure 6:** Depth wise  $(\Delta TA + \Delta Ca + \Delta Mg) / \Delta SO_4^{2-}$  ratios of U1445B and U1446B. Dotted lines indicate ratios of OSR and AOM.

**Supplementary Tables**

**Supplementary Table 1:** Concentrations and isotope ratios of various head space gases of cores U1445A&B and U1446A&B. HS and VAC stands for headspace and void gas respectively.

**Supplementary Table 2:** Concentrations and isotope ratios of various dissolved components in the pore-waters of U1445A&B and U1446A&B.

**Supplementary Table 3:** TIC, TOC and TN contents of U1445A and U1446A.

**Supplementary Table 4:** Depth wise porosity data of U1445B and U1446B.

Figure 1:

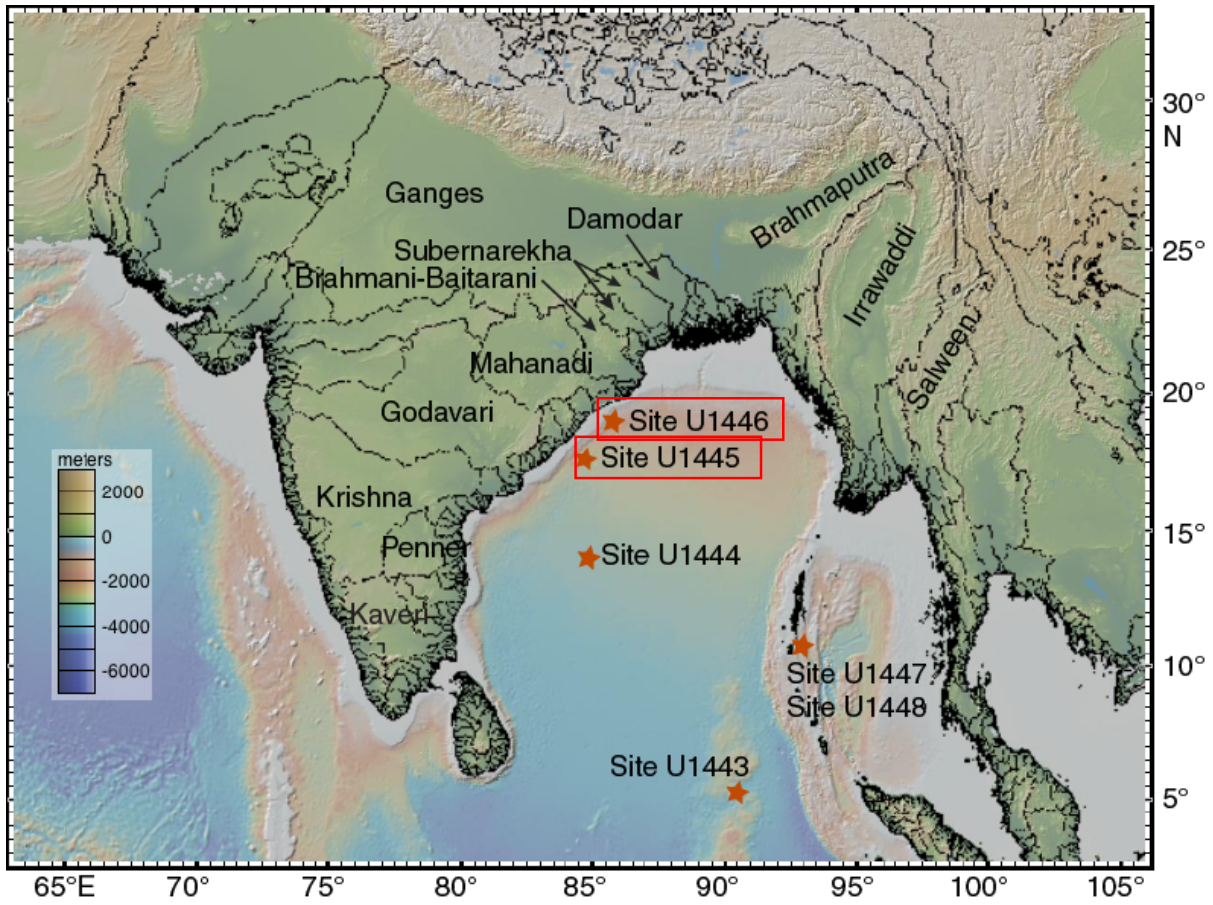


Figure-2:

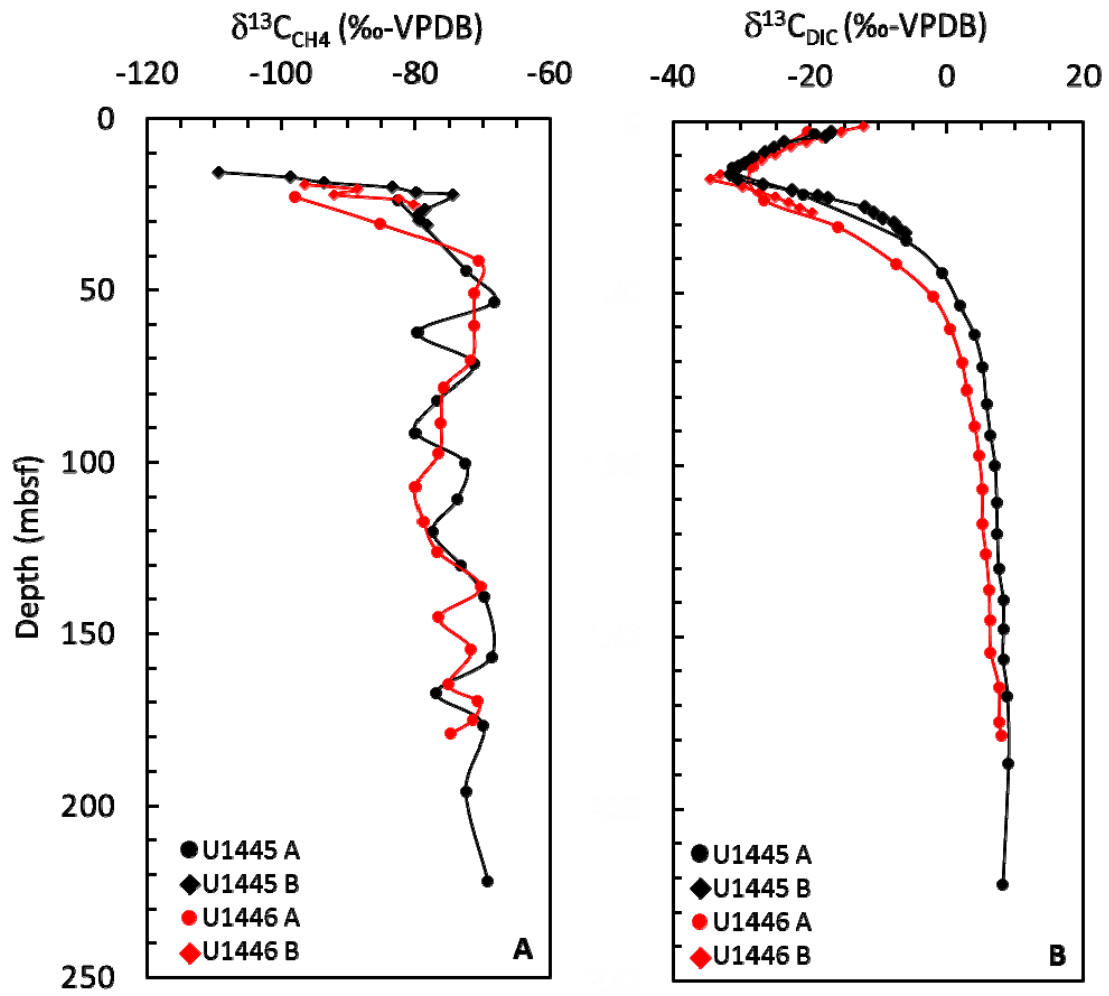


Figure 3:

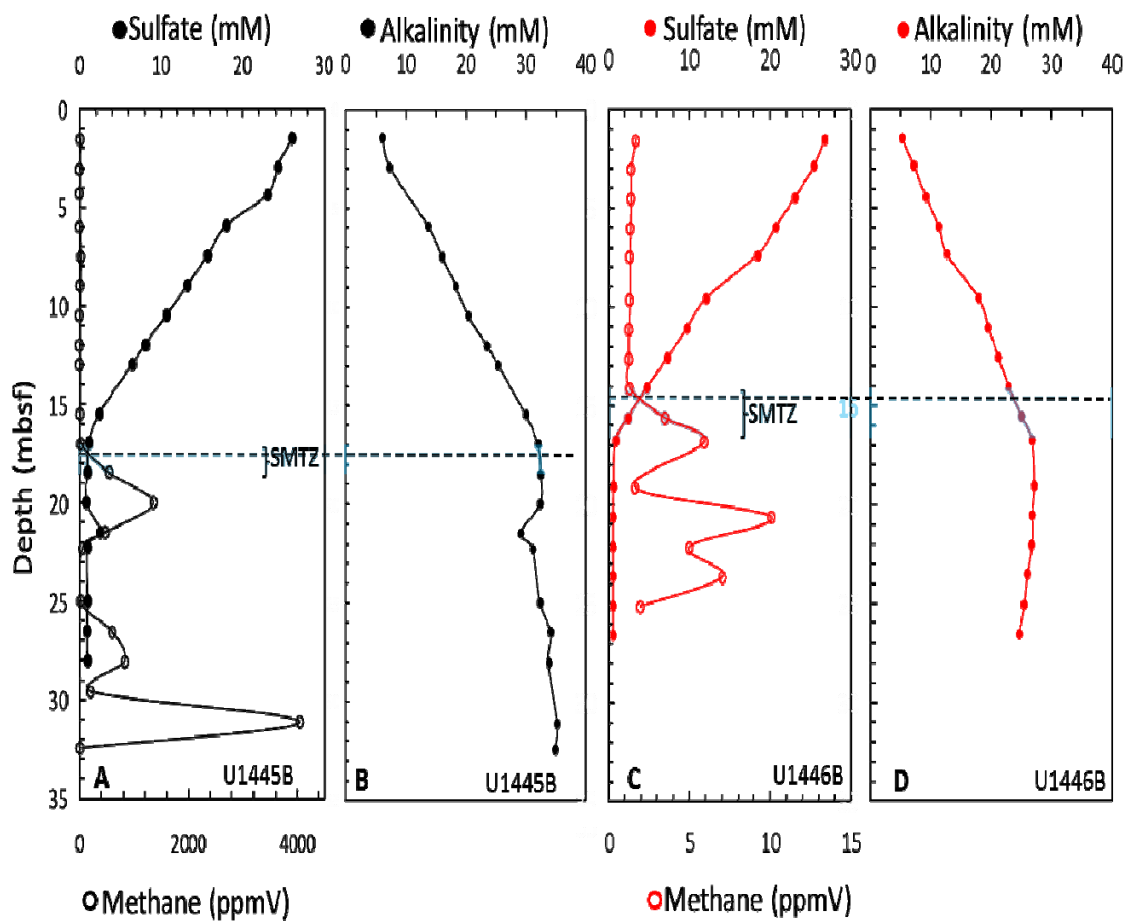


Figure 4:

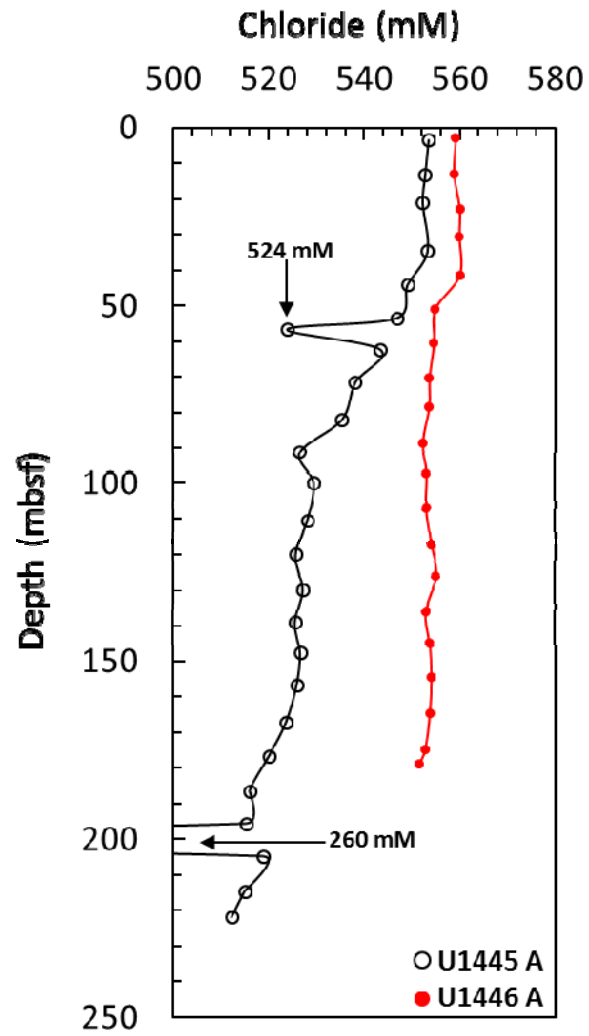


Figure 5:

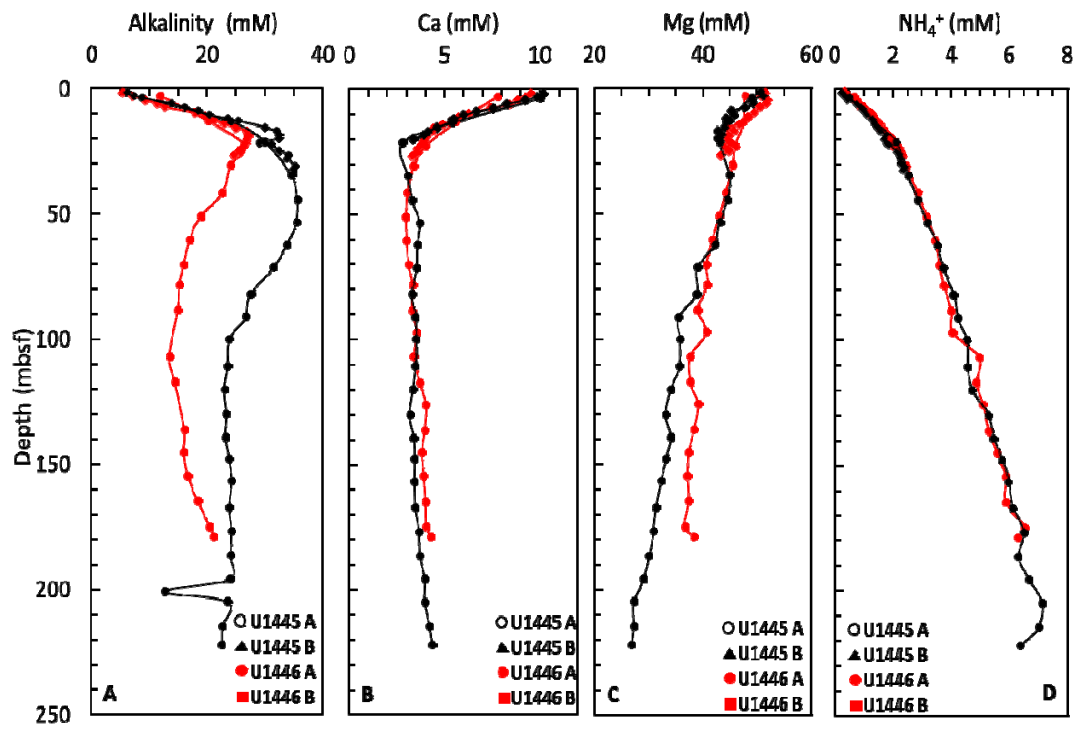
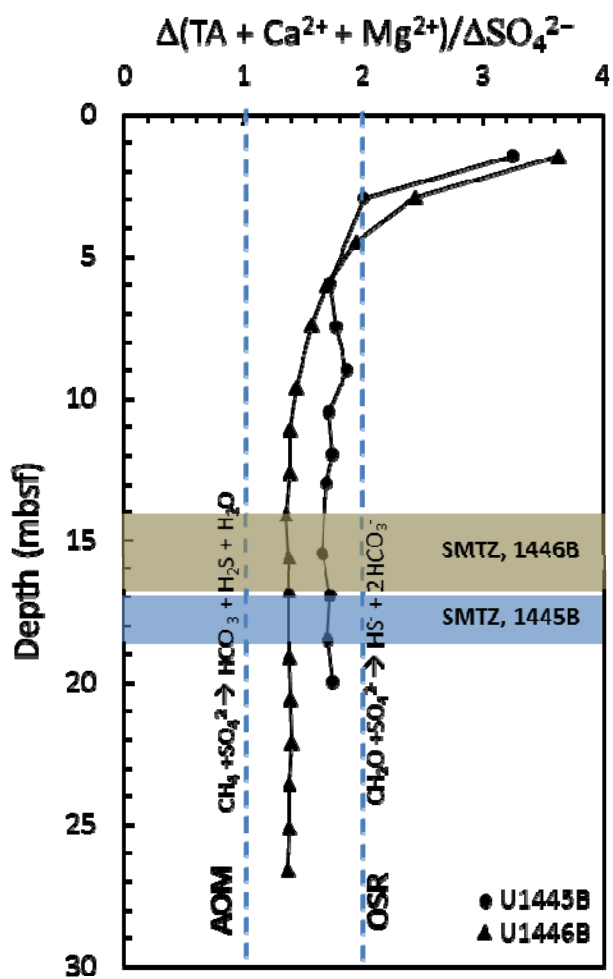




Figure 6:



Supplementary Table 1										
EXP-353 U1445A head space gas concentrations and isotope ratios										
Sl. No	Core	Type	Sect	Depth (mbsf)	Test code	CH <sub>4</sub> (ppmv)	C <sub>2</sub> H <sub>6</sub> (ppmv)	C <sub>3</sub> H <sub>8</sub> (ppmv)	H <sub>2</sub> S (ppmv)	δ <sup>13</sup> C <sub>CH4</sub> (‰-VPDB)
1	1	H	5	6.0	HS	2.1	BDL	BDL	NA	BDL
2	2	H	7	15.7	HS	2.5	BDL	BDL	NA	BDL
3	3	H	6	23.9	HS	12462.5	1.0	BDL	NA	-82.5
4	4	H	7	34.8	HS	4846.5	BDL	BDL	NA	NA
5	5	H	7	44.3	HS	9340.0	BDL	BDL	NA	-72.5
6	6	H	7	53.5	HS	2066.3	BDL	BDL	NA	-68.4
7	6	H	7	54.3	VAC	80896.7	BDL	BDL	23.2	NA
8	7	H	7	62.3	HS	1151.9	BDL	BDL	NA	-79.7
9	8	H	2	65.2	VAC	43995.9	BDL	BDL	1454.2	NA
10	8	H	7	71.6	HS	717.1	BDL	BDL	NA	-71.4
11	9	H	7	81.4	VAC	372929.9	BDL	BDL	1058.3	NA
12	9	H	8	82.1	HS	196.4	BDL	BDL	NA	-76.8
13	10	H	1	83.7	VAC	200413.4	BDL	BDL	677.1	NA
14	10	H	2	84.8	VAC	42426.8	BDL	BDL	76.1	NA
15	10	H	7	91.3	HS	960.8	BDL	BDL	NA	-80.0
16	11	H	5	98.3	VAC	527899.5	BDL	BDL	74.5	NA
17	11	H	7	100.2	HS	287.8	BDL	BDL	NA	-72.6
18	12	H	8	110.9	HS	492.9	BDL	BDL	NA	-73.8
19	13	H	3	115.0	VAC	515.0	BDL	BDL	73.0	NA
20	13	H	6	119.4	VAC	10078.3	BDL	BDL	70.7	NA
21	13	H	7	120.1	HS	1461.1	BDL	BDL	NA	-77.6
22	14	H	8	130.1	HS	634.7	BDL	BDL	NA	-73.3

23	15	H	7	139.4	HS	600.4	BDL	BDL	NA	-69.8
24	15	H	7	140.1	VAC	13898.5	BDL	BDL	74.5	NA
25	16	H	6	147.2	VAC	213989.2	BDL	BDL	74.2	NA
26	16	H	7	147.9	HS	1054.9	BDL	BDL	NA	NA
27	17	H	6	156.8	HS	2154.6	0.3	BDL	NA	-68.7
28	18	H	3	162.5	VAC	10833.0	BDL	BDL	76.7	NA
29	18	H	7	167.3	HS	3079.1	0.8	BDL	NA	-76.9
30	19	H	7	176.8	HS	1680.4	0.5	BDL	NA	-69.9
31	20	H	7	186.6	HS	2274.1	1.3	BDL	NA	NA
32	21	H	7	195.7	HS	3032.9	1.2	BDL	NA	-72.6
33	22	H	7	204.9	HS	1105.8	0.2	BDL	NA	NA
34	23	H	3	209.9	VAC	256212.7	BDL	BDL	72.7	NA
35	23	H	7	214.7	HS	1322.4	0.6	BDL	NA	NA
36	24	H	6	222.1	HS	2149.7	1.3	BDL	NA	-69.2
EXP-353 U1445B head space gas concentrations and isotope ratios										
Sl. No	Core	Type	Sect	Depth (mbsf)	Test code	CH <sub>4</sub> (ppmv)	C <sub>2</sub> H <sub>6</sub> (ppmv)	C <sub>3</sub> H <sub>8</sub> (ppmv)	H <sub>2</sub> S (ppmv)	δ <sup>13</sup> C <sub>CH4</sub> (‰-VPDB)
1	1	H	2	1.5	HS	8.7	BDL	BDL	NA	BDL
2	1	H	3	3.0	HS	1.9	BDL	BDL	NA	BDL
3	1	H	3	4.3	HS	1.9	BDL	BDL	NA	BDL
4	2	H	2	6.0	HS	1.5	BDL	BDL	NA	BDL
5	2	H	3	7.5	HS	21.7	BDL	BDL	NA	BDL
6	2	H	4	9.0	HS	9.8	BDL	BDL	NA	BDL
7	2	H	5	10.5	HS	1.7	BDL	BDL	NA	BDL
8	2	H	6	12.0	HS	1.7	BDL	BDL	NA	BDL
9	2	H	7	13.0	HS	1.3	BDL	BDL	NA	BDL

10	3	H	2	15.5	HS	4.9	BDL	BDL	NA	BDL
11	3	H	3	17.0	HS	25.9	BDL	BDL	NA	-109.4
12	3	H	4	18.5	HS	549.2	BDL	BDL	NA	-98.7
13	3	H	5	20.0	HS	1356.6	BDL	BDL	NA	-93.7
14	3	H	6	21.5	HS	471.9	BDL	BDL	NA	-83.4
15	3	H	7	22.3	HS	46.5	BDL	BDL	NA	-79.9
16	4	H	2	25.0	HS	16.1	BDL	BDL	NA	-74.6
17	4	H	3	26.6	HS	599.6	BDL	BDL	NA	NA
18	4	H	4	28.1	HS	825.9	BDL	BDL	NA	-78.6
19	4	H	5	29.6	HS	206.6	BDL	BDL	NA	-79.6
20	4	H	6	31.1	HS	4051.4	BDL	BDL	NA	-79.3
21	4	H	7	32.5	HS	10.9	BDL	BDL	NA	-78.3
EXP-353 U1446A head space gas concentrations and isotope ratios										
Sl. No	Core	Type	Sect	Depth (mbsf)	Test code	CH <sub>4</sub> (ppmv)	C <sub>2</sub> H <sub>6</sub> (ppmv)	C <sub>3</sub> H <sub>8</sub> (ppmv)	H <sub>2</sub> S (ppmv)	δ <sup>13</sup> C <sub>CH4</sub> (‰-VPDB)
1	1	H	3	3.0	HS	14.4	21.89	22.97	NA	BDL
2	2	H	7	13.1	HS	6.5	8.82	9.93	NA	BDL
3	3	H	7	22.8	HS	395.4	6.86	6.9	NA	-98.0
4	4	H	6	30.8	HS	84.3	BDL	BDL	NA	-85.2
5	5	H	7	41.6	HS	496.7	BDL	BDL	NA	-70.7
6	6	H	8	51.1	HS	973.8	BDL	BDL	NA	-71.3
7	7	H	8	60.5	HS	367.8	BDL	BDL	NA	-71.4
8	7	H	8	60.5	HS	1517.4	BDL	BDL	NA	NA
9	8	H	4	65.5	VAC	158566.2	BDL	BDL	76.78	NA
11	8	H	7	70.4	HS	NA	BDL	BDL	NA	-71.8

12	9	H	8	78.3	HS	3.7	BDL	BDL	NA	-75.8
13	10	H	8	88.6	HS	43.4	BDL	BDL	NA	-76.3
14	11	H	7	97.3	HS	32.1	BDL	BDL	NA	-76.6
15	12	H	7	107.1	HS	71.3	BDL	BDL	NA	-80.1
16	13	H	7	117.3	HS	102.9	BDL	BDL	NA	-78.9
17	14	H	7	126.0	HS	5.3	BDL	BDL	NA	-76.8
18	15	H	7	136.4	HS	86.7	BDL	BDL	NA	-70.4
19	16	H	7	145.3	HS	3.3	BDL	BDL	NA	-76.6
20	17	H	8	154.7	HS	10.3	BDL	BDL	NA	-71.8
21	18	H	8	164.8	HS	15.0	BDL	BDL	NA	-75.2
22	18	H	8	164.8	VAC	122119.4	BDL	BDL	78.48	NA
23	19	F	4	169.8	HS	1.8	BDL	BDL	NA	-70.8
24	20	F	2	172.9	VAC	43322.2	BDL	BDL	72.33	NA
25	20	F	4	175.0	HS	30.5	BDL	BDL	NA	-71.6
26	21	F	4	179.1	HS	37.7	BDL	BDL	NA	-74.9
EXP-353 U1446B head space gas concentrations and isotope ratios										
Sl. No	Core	Type	Sect	Depth (mbsf)	Test code	CH <sub>4</sub> (ppmv)	C <sub>2</sub> H <sub>6</sub> (ppmv)	C <sub>3</sub> H <sub>8</sub> (ppmv)	H <sub>2</sub> S (ppmv)	δ <sup>13</sup> C <sub>CH4</sub> (‰-VPDB)
1	1	H	2	1.5	HS	1.7	BDL	BDL	NA	BDL
2	1	H	3	3.0	HS	1.4	BDL	BDL	NA	BDL
3	1	H	4	4.5	HS	1.4	BDL	BDL	NA	BDL
4	1	H	5	6.0	HS	1.4	BDL	BDL	NA	BDL
5	1	H	6	7.4	HS	1.3	BDL	BDL	NA	BDL
6	2	H	2	9.6	HS	1.3	BDL	BDL	NA	BDL

	7	2	H	3	11.1	HS	1.3	BDL	BDL	NA	BDL
	8	2	H	4	12.6	HS	1.2	BDL	BDL	NA	BDL
	9	2	H	5	14.1	HS	1.3	BDL	BDL	NA	BDL
	10	2	H	6	15.6	HS	3.5	BDL	BDL	NA	BDL
	11	2	H	7	16.8	HS	5.9	BDL	BDL	NA	BDL
	12	3	H	2	19.1	HS	1.7	BDL	BDL	NA	-96.4
	13	3	H	3	20.6	HS	10.1	BDL	BDL	NA	-88.6
	14	3	H	4	22.1	HS	5.0	BDL	BDL	NA	-92.1
	15	3	H	5	23.6	HS	7.0	BDL	BDL	NA	-82.3
	16	3	H	6	25.1	HS	2.0	BDL	BDL	NA	-80.2
	BDL: Below detection limit										
	NA: Not analyzed.										

**Supplementary Table 2:** Concentrations and isotope ratios of various dissolved components in the pore-waters of U1445A&B and U1446A&B.  
EXP-353 U1445A Pore water concentrations

Sr. No	Core	Type	Section	Depth (mbsf)	pH	Alk (mM)	Cl <sup>-</sup> (mM)	SO <sub>4</sub> <sup>2-</sup> (mM)	Ca (mM)	Mg (mM)	NH <sub>4</sub> <sup>-</sup> (mM)	δ <sup>13</sup> C <sub>DIC</sub> (‰-VPDB)
1	1	H	4	3.5	7.5	8.7	553.6		10.1	49.1	0.49	-19.4
2	2	H	6	13.32	7.7	24.1	552.9	8.0	5.5	44.3	1.37	-31.2
3	3	H	5	21.26	7.6	30.0	552.4	0.9	2.8	43.2	2.10	-21.0
4	4	H	6	34.76	7.6	34.6	553.4	0.9	3.1	44.9	2.53	-6.0
5	5	H	6	44.28	7.7	35.7	549.1	0.9	3.3	44.5	2.86	-0.6
6	6	H	6	53.48	7.6	35.5	546.9	0.9	3.7	43.1	3.18	1.9
7	7	H	2	56.59	NA	NA	524.0	NA	NA	NA	NA	NA
8	7	H	6	62.28	7.8	33.8	543.5	0.9	3.6	42.2	3.53	4.1
9	8	H	6	71.5	7.6	31.5	538.3	0.9	3.5	39.0	3.73	5.3
11	9	H	7	82.06	7.6	27.5	535.4	0.8	3.3	38.9	4.10	5.8
12	10	H	6	91.28	7.6	26.6	526.6	0.8	3.5	35.5	4.23	6.4
13	11	H	6	100.1	7.7	23.9	529.6	0.8	3.5	35.8	4.54	7.1
14	12	H	7	110.8	7.6	23.5	528.2	0.8	3.5	35.7	4.57	7.3
15	13	H	6	120.09	7.7	23.0	525.7	0.9	3.4	34.1	4.72	7.4
16	14	H	7	130.04	7.7	23.3	527.3	0.9	3.2	33.2	5.29	7.6
17	15	H	6	139.31	7.7	23.2	525.7	0.8	3.4	34.1	5.47	8.3
18	16	H	6	147.86	7.6	23.8	526.7	0.9	3.4	33.2	5.74	8.3
19	17	H	5	156.73	7.7	24.2	526.0	0.8	3.4	32.3	5.98	8.3
20	18	H	6	167.25	7.6	23.8	523.7	0.8	3.5	31.4	6.14	8.9
21	19	H	6	176.78	7.8	24.2	520.1	0.9	3.7	30.9	6.50	NA
22	20	H	6	186.53	7.6	24.1	516.1	0.8	3.7	30.1	6.32	9.1
23	21	H	6	195.66	7.6	24.0	515.4	0.8	4.0	29.1	6.68	NA
24	22	H	3	200.62	8.1	12.6	260.2	NA	NA	NA	NA	NA

25	22	H	6	204.87	7.8	23.5	518.9	0.9	4.0	27.3	7.13	NA	
26	23	H	6	214.69	7.7	22.7	515.1	0.9	4.2	27.3	7.01	NA	
27	24	H	5	222.02	7.6	22.6	512.3	0.8	4.4	26.9	6.37	8.3	
EXP-353 U1445B Pore water concentrations													
Sr. No	Core	Type	Section	Depth (mbsf)	pH	Alk (mM)	Cl <sup>-</sup> (mM)	SO <sub>4</sub> <sup>2-</sup> (mM)	Ca (mM)	Mg (mM)	NH <sub>4</sub> <sup>-</sup> (mM)	δ <sup>13</sup> C <sub>DIC</sub> (‰-VPDB)	
1	1	H	1	1.48	7.47	6.103	541.7	26.1	10.2	50.7	0.25	NA	
2	1	H	2	2.93	7.556	7.284	531.6	24.3	9.9	51.1	0.35	-17.0	
3	1	H	3	4.36	NA	NA	NA	23.1	9.2	49	0.45	-17.8	
4	2	H	1	5.95	7.539	13.752	550.6	18.0	8.2	49.3	0.74	-23.9	
5	2	H	2	7.48	7.592	16.064	551.4	15.7	7.6	47.7	0.90	-25.2	
6	2	H	3	8.98	7.655	18.373	553.5	13.2	6.6	45.2	1.02	-26.7	
7	2	H	4	10.48	7.58	20.419	548.9	10.7	6.0	45.8	1.11	-28.3	
8	2	H	5	11.98	7.72	23.512	549.9	8.1	5.5	44.3	1.29	-29.4	
9	2	H	6	12.97	7.753	25.386	NA	6.5	5.3	44.8	1.35	-30.3	
10	3	H	1	15.48	7.934	29.968	550.9	2.5	4.6	44	1.46	-31.6	
11	3	H	2	16.98	7.831	32.008	551.7	1.2	4.1	42.7	1.58	-30.3	
12	3	H	3	18.48	7.843	32.481	551.8	1.0	3.9	43.5	1.76	-26.9	
13	3	H	4	19.98	7.748	32.391	518.0	0.9	3.4	42.8	1.70	-22.8	
14	3	H	5	21.48	7.729	29.129	538.0	2.5	NA	NA	1.78	-18.9	
15	3	H	6	22.28	7.669	31.181	548.4	1.0	2.7	43.4	1.88	-17.4	
16	4	H	1	25.00	7.818	32.388	495.0	1.0	2.6	45.4	2.11	-12.0	
17	4	H	2	26.50	7.83	34.15	548.3	1.0	2.8	44.9	2.21	-10.7	
18	4	H	3	28.05	7.878	33.804	545.9	1.0	2.7	43.4	2.27	-9.4	



19	4	H	4	29.56	NA	NA	546.6	BDL	2.9	43.8	2.29	-7.8	
20	4	H	5	31.11	7.823	35.212	548.1	BDL	3.0	44.9	2.40	-7.0	
21	4	H	6	32.45	7.811	34.905	542.8	BDL	3.0	44.1	2.35	-6.2	
EXP-353 U1446A Pore water concentrations													
Sr. No	Core	Type	Section	Depth	pH	Alk	Cl <sup>-</sup>	SO <sub>4</sub> <sup>2-</sup>	Ca	Mg	NH <sub>4</sub> <sup>+</sup>	δ <sup>13</sup> C <sub>DIC</sub>	
				(mbsf)		(mM)	(mM)	(mM)	(mM)	(mM)	(mM)	(‰-VPDB)	
1	1	H	2	2.95	7.5	11.9	559.2	19.7	7.8	47.8	0.68	-20.4	
2	2	H	6	13.05	7.7	20.2	558.8	8.6	5.6	47.6	1.36	-28.4	
3	3	H	6	22.75	7.6	26.4	560.0	0.6	4.0	46.0	2.03	-26.9	
4	4	H	5	30.75	7.6	24.0	560.0	0.6	3.4	45.5	2.47	-15.9	
5	5	H	6	41.52	7.6	22.7	560.0	0.6	3.0	44.2	2.86	-7.4	
6	6	H	7	51.04	7.6	18.9	554.9	0.6	3.0	43.1	3.17	-2.1	
7	7	H	7	60.43	7.6	17.0	554.6	0.6	3.0	41.7	3.46	0.5	
8	8	H	7	70.34	7.6	16.0	553.7	0.6	3.1	40.7	3.61	2.2	
9	9	H	7	78.28	7.6	15.2	553.6	0.6	3.3	40.9	3.75	3.0	
10	10	H	7	88.49	7.6	14.9	552.2	0.6	3.3	39.1	4.02	4.1	
11	11	H	6	97.22	NA	NA	553.1	0.6	3.5	40.7	4.07	4.7	
12	12	H	6	107.03	7.7	13.5	553.0	0.6	3.4	37.7	4.98	5.2	
13	13	H	6	117.2	7.6	14.4	554.1	0.6	3.7	37.7	4.89	5.2	
14	14	H	6	125.94	NA	NA	555.2	0.6	4.0	39.2	5.11	5.7	
15	15	H	6	136.31	7.5	16.1	553.0	0.6	4.0	38.4	5.31	6.2	
16	16	H	6	145.15	7.4	16.0	553.7	0.6	3.8	37.4	5.58	6.3	
17	17	H	7	154.6	7.6	16.7	554.0	0.7	3.9	37.2	5.89	6.4	
18	18	H	7	164.73	7.5	18.4	553.7	0.6	4.0	37.4	5.88	7.6	
19	20	F	3	174.94	7.4	20.5	552.7	0.6	4.0	36.7	6.54	7.7	
20	21	F	3	178.95	7.4	21.1	551.5	0.6	4.3	38.4	6.30	8.0	

EXP-353 U1446B Pore water concentrations												
Sr. No	Core	Type	Section	Depth (mbsf)	pH	Alk (mM)	Cl <sup>-</sup> (mM)	SO <sub>4</sub> <sup>2-</sup> (mM)	Ca (mM)	Mg (mM)	NH <sub>4</sub> <sup>+</sup> (mM)	δ <sup>13</sup> C <sub>DIC</sub> (‰-VPDB)
1	1	H	1	1.45	7.5	5.3	551.7	26.8	9.6	51.4	0.35	-12.2
2	1	H	2	2.85	7.6	7.2	548.9	25.5	9.3	50.8	0.48	-15.5
3	1	H	3	4.45	7.5	9.3	545.9	23.1	8.8	51.7	0.69	-18.3
4	1	H	4	5.95	7.6	11.3	549.0	20.7	8.4	51.6	0.83	-20.5
5	1	H	5	7.35	7.6	12.7	551.5	18.5	7.4	50.5	0.99	-22.9
6	2	H	1	9.55	7.6	17.9	551.4	12.1	6.3	49.5	1.24	-25.1
7	2	H	2	11.05	7.7	19.6	553.6	9.7	5.7	48.3	1.30	-27.1
8	2	H	3	12.55	7.7	21.2	551.4	7.3	5.4	47.9	1.43	-28.9
9	2	H	4	14.05	7.7	22.9	553.6	4.8	4.9	46.7	1.54	-31.0
10	2	H	5	15.55	7.7	25.0	522.1	2.5	4.4	44.4	1.57	-33.0
11	2	H	6	16.75	7.8	26.8	554.9	0.9	4.3	45.8	1.72	-34.5
12	3	H	1	19.05	7.8	27.1	554.7	0.6	4.0	44.6	1.90	-29.7
13	3	H	2	20.55	7.8	26.8	NA	0.6	3.9	44.5	1.98	-27.5
14	3	H	3	22.05	7.7	26.7	555.5	0.6	3.8	45.2	2.09	-25.2
15	3	H	4	23.55	7.7	26.0	557.1	0.6	3.6	44.1	2.19	-23.2
16	3	H	5	25.05	7.7	25.5	NA	0.6	3.6	44.8	2.25	-21.6
17	3	H	6	26.55	7.8	24.7	556.5	0.6	3.3	43.3	2.30	-19.7
NA: Not analysed												
BDL: Below detection limit												

<b>Supplementary Table 3</b>							
EXP-353 U1445A TOC, TIC and TN contents.							
Sr. No	Core	Type	Sect	Depth	TIC	Nitrogen	TOC
				(mbsf)	(wt. %)	(wt. %)	(wt. %)
1	1	H	1	1.0	0.2	0.32	1.49
2	1	H	3	4.3	2.4	NA	NA
3	1	H	5	6.2	3.0	NA	NA
4	2	H	2	8.8	1.3	0.41	2.03
5	2	H	4	11.8	2.2	NA	NA
6	2	H	6	14.8	0.9	NA	NA
7	3	H	2	18.2	0.3	0.25	1.12
8	3	H	4	21.2	2.9	NA	NA
9	3	H	6	24.2	2.6	NA	NA
10	4	H	2	28.5	1.2	0.22	1.01
11	4	H	4	31.6	0.2	NA	NA
12	4	H	6	34.7	0.7	NA	NA
13	5	H	2	37.9	1.5	0.29	1.63
14	5	H	4	40.9	1.4	NA	NA
15	5	H	6	43.9	0.4	NA	NA
16	6	H	2	47.1	0.6	0.25	1.07
17	6	H	4	50.0	1.7	NA	NA

18	6	H	6	52.9	0.5	NA	NA
19	7	H	2	56.8	1.9	0.21	1.03
20	7	H	4	59.5	0.6	NA	NA
21	7	H	6	62.1	0.6	NA	NA
22	8	H	2	65.5	0.2	0.28	1.47
23	8	H	4	68.2	0.4	NA	NA
24	8	H	6	71.1	1.1	NA	NA
25	9	H	2	74.8	0.3	0.27	1.17
26	9	H	4	77.5	1.8	NA	NA
27	9	H	6	80.3	2.5	NA	NA
28	10	H	2	84.6	0.6	0.23	0.95
29	10	H	4	87.5	1.4	NA	NA
30	10	H	6	90.3	1.2	NA	NA
31	11	H	2	94.4	0.7	0.29	1.39
32	11	H	4	96.8	0.7	NA	NA
33	11	H	6	99.2	6.1	NA	NA
34	12	H	2	102.7	0.8	0.23	1.12
35	12	H	4	105.4	0.3	NA	NA
36	12	H	6	108.1	0.7	NA	NA
37	13	H	2	113.4	0.2	0.26	1.07
38	13	H	4	116.3	0.9	NA	NA
39	13	H	6	119.9	0.3	NA	NA
40	14	H	3	123.5	1.5	0.31	1.54
41	14	H	5	126.7	0.3	NA	NA
42	14	H	7	128.7	1.5	NA	NA

43	15	H	2	132.8	0.5	0.28	1.15
44	15	H	4	135.7	0.9	NA	NA
45	15	H	6	138.7	0.6	NA	NA
46	16	H	2	141.8	0.1	0.34	1.36
47	16	H	4	144.6	0.5	NA	NA
48	17	H	2	151.8	0.3	0.28	1.11
49	17	H	4	155.2	0.3	NA	NA
50	17	H	5	156.6	0.5	NA	NA
51	18	H	2	161.3	0.3	0.44	2.26
52	18	H	4	164.1	0.5	NA	NA
53	18	H	6	166.8	0.3	NA	NA
54	19	H	2	170.6	0.4	0.21	0.80
55	19	H	4	173.3	1.6	NA	NA
56	19	H	6	176.2	0.4	NA	NA
57	20	H	2	180.2	0.2	NA	NA
58	20	H	4	183.1	0.4	NA	NA
59	20	H	6	186.0	0.3	NA	NA
60	21	H	2	189.3	0.4	0.39	1.84
61	21	H	4	192.3	0.5	NA	NA
62	21	H	6	194.6	0.3	NA	NA
63	22	H	2	199.3	0.7	0.44	2.10
64	22	H	4	201.6	0.5	NA	NA
65	22	H	6	204.4	0.3	NA	NA
66	23	H	2	208.4	0.3	0.33	1.31
67	23	H	4	211.3	0.3	NA	NA

68	23	H	6	213.9	0.8	NA	NA
69	24	H	2	217.0	0.3	0.33	1.48
70	24	H	4	219.7	0.6	NA	NA
71	24	H	6	222.4	0.9	NA	NA
EXP-353 U1446A TOC, TIC and TN contents.							
Sr. No	Core	Type	Sect	Depth (mbsf)	TIC (wt. %)	Nitrogen (wt. %)	TOC (wt. %)
1	1	H	2	2.2	0.2	0.31	1.35
2	2	H	2	7.0	2.4	NA	NA
3	2	H	4	10.0	1.7	0.32	1.57
4	2	H	6	13.0	1.1	NA	NA
5	3	H	2	16.4	0.4	0.33	1.39
6	3	H	4	19.4	0.7	NA	NA
7	3	H	6	22.4	0.5	0.35	1.58
8	4	H	2	25.1	0.2	NA	NA
9	4	H	4	28.1	0.4	0.25	1.05
10	4	H	6	31.1	1.0	NA	NA
11	5	H	2	34.7	1.3	0.38	1.69
12	5	H	4	37.5	0.5	NA	NA
13	5	H	6	40.5	0.2	0.32	1.22
14	6	H	2	44.4	0.5	NA	NA
15	6	H	4	46.5	0.8	0.27	1.18
16	6	H	6	49.3	0.4	NA	NA

17	7	H	2	53.7	0.5	0.94	1.69
18	7	H	4	55.8	0.7	NA	NA
19	7	H	6	58.6	0.4	0.31	1.19
20	8	H	2	62.6	1.7	NA	NA
21	8	H	4	65.0	1.0	0.59	1.24
22	8	H	6	67.7	0.5	NA	NA
23	9	H	2	72.6	0.1	0.73	1.24
24	9	H	4	75.1	1.9	NA	NA
25	9	H	6	76.4	1.3	0.82	2.90
26	10	H	2	81.0	0.3	NA	NA
27	10	H	4	83.8	0.3	0.73	1.29
28	10	H	6	86.3	0.3	NA	NA
29	11	H	2	91.3	0.8	0.63	1.11
30	11	H	4	93.9	1.0	NA	NA
31	11	H	6	96.2	0.5	0.73	1.14
32	12	H	2	100.6	1.8	NA	NA
33	12	H	4	103.3	1.2	0.67	1.23
34	12	H	6	106.3	0.6	NA	NA
35	13	H	2	111.1	1.2	0.75	1.33
36	13	H	4	113.9	0.5	NA	NA
37	13	H	6	116.7	2.3	0.48	0.79
38	14	H	2	119.1	0.6	NA	NA
39	14	H	4	121.9	0.5	0.69	1.04
40	15	H	2	130.1	0.5	0.71	1.21
41	15	H	4	132.9	0.4	NA	NA

42	15	H	6	135.8	0.9	0.82	1.40
43	16	H	2	138.9	1.1	NA	NA
44	16	H	4	141.6	0.9	0.88	1.55
45	16	H	6	144.0	0.5	NA	NA
46	17	H	2	147.5	0.6	0.83	1.25
47	17	H	4	150.3	0.9	NA	NA
48	17	H	6	152.2	1.0	0.69	1.18
49	18	H	2	157.0	1.2	NA	NA
50	18	H	4	159.6	0.6	0.68	1.07
51	18	H	6	162.4	0.7	NA	NA
52	19	F	2	167.8	1.0	0.76	1.33
53	19	F	4	170.3	0.3	NA	NA
54	20	F	2	172.2	0.6	NA	NA
55	20	F	4	175.2	0.1	0.80	1.39
56	21	F	2	177.9	0.6	NA	NA
57	21	F	4	179.6	0.9	0.60	0.89
NA: Not analyzed							



<b>Supplementary Table 4</b>		
EXP-353 U1445B porosity data		
Depth	Porosity	
(mbsf)	(vol%)	
1.5	79.0	
2.9	78.5	
4.3	77.9	
6.0	77.3	
7.5	76.7	
9.0	76.1	
10.5	75.5	
12.0	74.9	
13.0	74.6	
15.5	73.6	
17.0	73.0	
18.5	72.4	
EXP-353 U1446B porosity data		
Depth	Porosity	
(mbsf)	(vol%)	
1.5	75.5	
3.0	75.1	
4.5	74.7	
6.0	74.2	
7.4	73.8	
9.6	73.2	

11.1	72.7	
12.6	72.3	
14.1	71.8	
15.6	71.4	
16.8	71.0	